UNIVERSITY OF CALIFORNIA SAN DIEGO

Brain Endothelial Nitric Oxide Mediates Increased Expression of Astrocyte-derived VEGF in the Pathogenesis of Cerebral Cavernous Malformations

A Thesis submitted in partial satisfaction of the
requirements for the degree Master of Science

in

Biology

by

Shady Ibrahim Soliman

Committee in charge:

Mark H. Ginsberg, Chair
Elizabeth Villa, Co-Chair
Aaron Coleman
Stacey Glasgow

2019

The Thesis of Shady Ibrahim Soliman is approved and it is acceptable in quality and form for publication on microfilm and electronically:

Co-Chair

Chair

University of California San Diego

2019

DEDICATION

In recognition of their endless support, altruism, and love, this thesis is dedicated to my mother, Martha Soliman, and my father, Ash Soliman.

TABLE OF CONTENTS

LIST OF FIGURES

ACKNOWLEDGEMENTS

This thesis would not have been possible without the exceptional support of others.

I would like to thank my chair Mark H. Ginsberg, co-chair Elizabeth Villa, Aaron Coleman, and Stacey Glasgow for serving on my committee. In particular, I would like to recognize Dr. Ginsberg for providing me this opportunity to do research in his lab. I thank you for your immense support and kindness, and greatly admire your spirit of inquiry. I would also like to acknowledge Miguel Lopez-Ramirez, my acting mentor, who has taught me how to navigate even the most difficult questions and to always pursue the next answer. Your motivation and determination continuously inspire me, and I thank you for your endless guidance and compassion. Furthermore, I would like to acknowledge Miguel Lopez-Ramirez's and Mark H. Ginsberg's support in the editing and revision of this thesis.

I would like to recognize Preston Hale and Angela Pham who tremendously contributed to this work, as well as the rest of our colleagues and collaborators who have helped acquire the data that is presented in this thesis. I would also like to acknowledge all of the members of the lab that provided their knowledge, support, and encouragement in my path towards becoming a better scientist. Finally, I would like to thank my family and friends for their unending love and support.

Chapter 2 and 3, in part, are currently being prepared for submission for publication of the material. Soliman, Shady; Hale, Preston; Pham, Angela; Lai, Catherine; Lagarrigue, Frederic; Sun, Hao; Ginsberg, Mark H. and Lopez-Ramirez, Miguel A. The thesis author is a coauthor of this material.

ABSTRACT OF THE THESIS

Brain Endothelial Nitric Oxide Mediates Increased Expression of Astrocyte-derived VEGF in the Pathogenesis of Cerebral Cavernous Malformations

by

Shady Ibrahim Soliman

Master of Science in Biology

University of California San Diego, 2019

Mark Howard Ginsberg, Chair
Elizabeth Villa, Co-Chair

Cerebral Cavernous Malformations (CCM) are central nervous system vascular anomalies that arise primarily due to loss-of-function mutations in *KRIT1, CCM2,* or *PDCD10* (CCM3). CCM are characterized by endothelial dysfunction and the loss of endothelial junctions, leading to grossly-dilated blood vessels and increased vascular permeability. Previous studies demonstrate that CCM are hypersensitive to angiogenesis due to the loss of an anti-angiogenic checkpoint and increased VEGF signaling. Here, we report that loss of PDCD10 in brain endothelial cells causes upregulation of eNOS in CCM lesions. Furthermore, elevated eNOS expression results in

increased secretion of NO, an important intercellular messenger in the CNS responsible for vascular remodeling and angiogenesis. To analyze the effect of upregulated eNOS and release of NO during CCM, we prepared co-culture studies using purified astrocytes and mouse brain microvascular endothelial cells (BMEC) harboring inactivated *Pdcd10* (*Pdcd10*^{ECKO}). Increased levels of eNOS in *Pdcd10*^{ECKO} BMEC induced upregulation of astrocyte-derived *Vegfa.* The increase in astrocyte-derived *Vegfa* mRNA was specific to the upregulation of eNOS because genetic inactivation of one copy of the *Nos3* gene in *Pdcd10*^{ECKO} BMEC was sufficient to prevent *Vegfa* upregulation in astrocytes. Moreover, upregulation of eNOS in *Pdcd10*^{ECKO} BMEC was correlated with HIF-1α protein stabilization in astrocytes during co-culture studies. These studies identify that increased expression of eNOS during CCM may lead to augmented levels of NO capable of stabilizing HIF-1α protein and inducing astrocyte-derived VEGF. Therefore, we propose the possibility that CCM lesion formation and progression can be exacerbated by the non-cell-autonomous release of VEGF from perivascular astrocytes.

ABBREVIATIONS

BEC – Brain endothelial cell

BBB – Blood-brain barrier

CCM – Cerebral Cavernous Malformations

GFAP – Glial fibrillary protein

KLF2 – Kruppel-like Factor 2

KLF4 – Kruppel-like Factor 4

eNOS – Endothelial nitric oxide synthase

NO – Nitric oxide

VEGF – Vascular endothelial growth factor

BMEC – Brain microvascular endothelial cell

HIF-1α - Hypoxia inducible factor – 1α

1. Introduction

1.1. Anatomy of the central nervous system vasculature

The central nervous system (CNS) makes up only 2% of the human body's mass, yet constitutes nearly 20% of the body's energy at rest.[1] Confined by its limited capacity for energy storage, the CNS is highly vascularized; forming a specialized network of blood vessels that provide oxygen and nutrients to CNS-resident cells. In the brain, blood enters through major arteries that converge at the circle of Willis located at the base of the brain, and exits through the cerebral veins and superior sagittal sinus.[2] Interposed between these two circulatory passages is the cerebral microvasculature, where most oxygen and nutrient transfer occurs. The cerebral microvasculature is composed of the following: 1) arterioles (15-75μm) that penetrate the cerebral tissue from the basilar brain 2) brain capillaries (4-10μm) that are ~50-100 times tighter than peripheral capillaries and branch out to encompass a large surface area where major exchange between blood and the brain occurs;[3] and 3) venules (10-100μm) that contain a looser arrangement of tight junctions and are the main area of leukocyte infiltration.[4]

1.2. Structure and components of the central nervous system microvasculature

Over a century ago, it was first observed that the systemic injection of water-soluble trypan blue dye stained several tissues in the body, but failed to stain the brain.[1] Those initial experiments led to the idea of a cellular barrier that restricts the free entrance of hydrophilic molecules from blood to brain and brain to blood. While Lewandowsky introduced the term "blood-brain barrier" (BBB) by 1900, it was not until the late 1960s with the development of electron microscopy techniques that the anatomical localization of the BBB was identified by Reese, Karnovsky, and Brightman.[5] In two independent studies, their collective observations established that the BBB is

localized at the level of the brain endothelial cells (BEC) and due to the presence of highly complex tight junctions along the brain capillaries.[5] More recently, the CNS vasculature has been considered a cellular complex-structure termed the "neurovascular unit" that comprises a dynamic communication and feedback network of cells including BECs, pericytes, astrocytes, microglia, smooth muscles, and neurons, as well as the extracellular matrix and endothelial glycocalyx. **(Figure 1)**.[6] Importantly, it is the molecular and cellular interactions among the neurovascular unit that allow a coordinated response necessary to maintain a functional BBB.[7,8] However, it has been reported that the neurovascular unit can be uncoupled due to stress and pathological conditions such as neurodegenerative diseases, neuroinflammation, and vascular abnormalities, among others.[3,6,9,10]

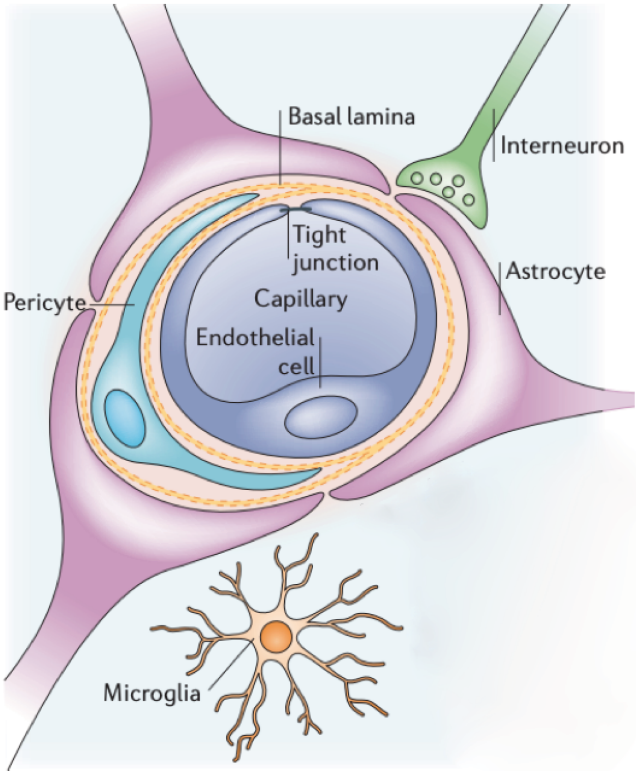

Figure 1. Neurovascular Unit. The neurovascular unit is composed of CNS-resident neurons and glia that interact with vascular cells to support normal vascular functions. The BBB forms at the center of the neurovascular unit through tight endothelial interactions. Adapted with modifications from "Astrocyte–endothelial interactions at the blood–brain barrier" by J. Abbott, L. Ronnback, E. Hansson, *Nature Reviews Neuroscience*, 2006, vol. 7, p. 41-53

1.2.1 Brain microvascular endothelial cells

Blood vessels of the CNS are composed of a continuous layer of BECs that shape the tubular vessel walls. BECs act as "gatekeepers" by allowing the entrance of nutrients such as glucose, amino acids, and other blood-borne substances such as insulin. At the same time, the BECs remove waste products out of the CNS for proper neuronal function.[11,12] BECs can also act as a "physical barrier" by the presence of complex intercellular junctions and their lack of fenestrations that maintain the integrity of the BBB.[1,9,13] The intercellular junctions in BECs are comprised of both tight junctions and adherens junctions which consist of transmembrane proteins that seal the intercellular space between BECs.[3,9,13] Both adherens and tight junctions indirectly interact with the cytoskeleton by a number of cytoplasmic adaptors and scaffolding proteins to regulate and strengthen the cell-cell junctions **(Figure 2)**.[9,11] The firmly-sealed BECs prevent the paracellular movement of hydrophilic molecules, permitting the passage of only small lipophilic molecules <400 Daltons, such as ethanol, and the free diffusion of gases, such as oxygen, carbon dioxide, and nitric oxide.[14]

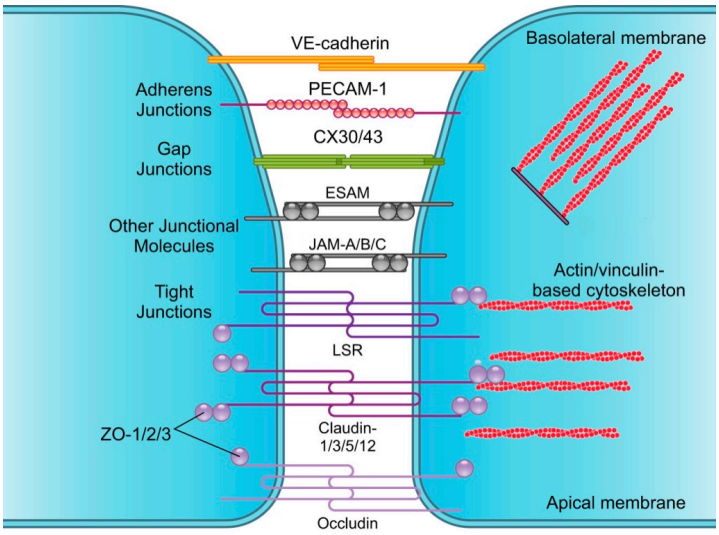

Figure 2. CNS Endothelial Cell Junctions. Adherens and tight junctions consist of transmembrane proteins that seal the intercellular space between BECs and interact with the cytoskeleton through cytoplasmic adaptors that can strengthen cell-cell interactions. Adapted from "Blood-Brain Barrier: From Physiology to Disease and Back" by M. Sweeney, Z. Zhao, A. Montane, A. Nelson, and B. Zlokovic, *Physiological Reviews*, 2018, vol. 99, p. 21-78

1.2.2 Pericytes

Pericytes are contractile mural cells that share a basement membrane with BECs. Perivascular pericytes are intermittently present throughout the entire brain vasculature, but found most frequently in the brain capillaries where they have been shown to regulate cerebral blood flow,[15] maintain BBB properties,[16] and promote blood vessel stabilization.[7]

1.2.3 Neurons

Neurons are specialized cells whose synapses transmit signals to the CNS vasculature by communication with interposed astrocytes.[6] Neurons are capable of communicating with brain capillaries through neurotransmitters in order to regulate cerebral flow and permit the movement of substrates across the endothelium, a process that has been termed *neurovascular coupling.*[6,17] In addition, neurons have been tied to vascular functions by facilitating tight junction maintenance[9] and angiogenesis[1] through vascular-neuronal cross-talk.

1.2.4 Astrocytes

Astrocytes serve as important glial cells in the CNS that maintain BBB functions[11] and regulate cerebral blood flow.[3] Astrocytes reside ~6-10μm from the outer surface of BECs and project their end-foot processes towards BECs and pericytes.[18,19,20] Cross-talk between the BECs and astrocytes occurs through various soluble secreted factors that get released by the perivascular endfeet of astrocytic glia into the basal lamina, where they can bind to receptors of BECs and induce signaling pathways.[9,11] Among these astrocyte-released factors are: angiotensin-1, transforming growth factor-β (TGF-β) and vascular endothelial growth factor (VEGF), which modulate multiple BBB properties.[3,7,9,21] During diseases that affect the CNS, astrocytes can become activated (astrogliosis) leading to morphological changes including an increase in glial

fibrillary acidic protein (GFAP)[22] and production of a wide range of molecules including growth factors, cytokines, chemokines, and reactive oxygen species that contribute to BBB breakdown.[3,10,22]

1.3. Vascular dysfunction in central nervous system diseases

Alterations in the cerebral vasculature can lead to progressive or permanent changes in BEC morphology and function that can contribute to uncoupling of the neurovascular unit, resulting in neurological diseases.[6] Moreover, recent studies suggest that cerebrovascular dysfunction may be an initiating trigger for neurological disorders and subsequent neurological disease manifestation.[3,9,10] For example, vascular dysfunction in Alzheimer disease has been reported to be a hallmark of this syndrome.[23] In this context, amyloid-beta (Aβ) peptide, the main component of amyloid plaques, can form deposits onto and around the cerebral vasculature leading to a decrease in cerebral blood flow, BEC dysfunction, and subsequent accumulation of neurotoxins, all of which can contribute to neuronal death.[24] In contrast, Cerebral Cavernous Malformations (CCMs) arise as a primary cause of BEC dysfunction that results in neurological disabilities as described below.[25]

1.4. The pathogenesis of cerebral cavernous malformations

CCMs are "mulberry"-like vascular anomalies that affect the CNS **(Figure 3)**.[26,27] CCMs are characterized by dilated blood-filled vessels within the venous-capillary vascular bed and are prone to hemorrhage. CCM lesions show marked BBB dysfunction and leakiness associated with changes in BEC morphology and function, which lead to the loss of tight and adherens junctions.[9] CCMs are found in ~0.5% of humans leading to risk of strokes, focal seizures, and neurological deficits.[28,29] Currently, no pharmacologic therapy exists for CCM, and malformations can only be

removed through surgical resectioning when possible.[29–31] CCMs occur as a sporadic (80% of patients) or familial form (20% of patients), and can be transmitted in an autosomal dominant pattern with incomplete penetrance and variable expressivity.[28,32] Sporadic forms of the disease typically result in a single lesion, while familial CCMs are characterized by multiple vascular lesions.[28,33] CCMs are associated with loss-of-function mutations of three genes: *KRIT1* (Krev1 interaction trapped gene 1, CCM1), *CCM2* (Cerebral cavernous malformation 2 protein), and *PDCD10* (Programmed cell death protein 10, CCM3).[34,35] The *KRIT1*$^{+/-}$ genotype is the most common cause of the familial form of CCM, while the *PDCD10*$^{+/-}$ genotype results in the most aggressive form of the disease.[33,36]

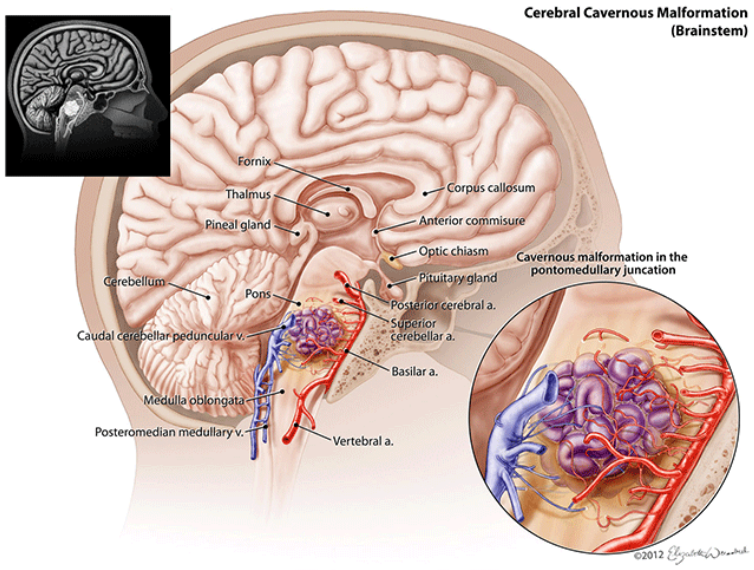

Figure 3. Cerebral Cavernous Malformations. CCMs are mulberry-shaped vascular aberrations that occur in the venous capillaries of the brain. Adapted from the Dartmouth-Hitchcock "Cerebrovascular Disease and Stroke Program" by R. Singer, 2014.

Moreover, analysis of the incomplete penetrance in CCM patients suggests that a Knudson two-hit mechanism is involved in the pathogenesis of the vascular abnormalities.[37] This mechanism proposes that the formation of CCM requires the complete loss of function of a CCM

gene on both alleles of affected cells. The loss of function in one allele (first hit) is inherited as a germline mutation and the loss of a second allele (second hit) would occur randomly in the CNS at any age, leading to the vascular abnormalities formed.[28] Heterogeneity of the CCM disease in patients with the same genetic mutation suggests that there may be other genes[38] or environmental factors that trigger disease onset and progression, and may contribute to variable expressivity of CCM.

1.5. Cellular and molecular mechanisms of cerebral cavernous malformations

Proteins encoded by the genes *KRIT1*, *CCM2*, and *PDCD10* play a major role in cardiovascular development and integrity[39–41] by forming a protein complex.[42,43] Our lab and others have shown that the CCM protein complex stabilizes endothelial cell-cell interactions by suppressing the activation of the RhoA-ROCK signaling pathway.[44] In addition, our group has shown that the loss of junctional integrity due to the loss-of-function of KRIT1 leads to increased WNT/b-catenin signaling and increased expression of b-catenin-driven genes such as VEGF-a.[45,46] Increased VEGF signaling could contribute to a dramatic disassembly of brain endothelial intercellular junctions and cerebrovascular dysfunction and leakiness.[10,36,46,47] Moreover, loss of endothelial KRIT1 suppresses the expression of a key angiogenic checkpoint protein, thrombospondin1 (*Thbs1*, which encodes TSP1).[36] In addition, the loss of TSP1 from the brain endothelium positively alters VEGF signaling and TSP1 replacement inhibits the augmented VEGF signaling and subsequent formation of CCM.[36]

Other studies have implicated additional angiogenic signaling pathways including expression of endothelial metalloproteinases,[48] loss of Notch signaling,[49] and increased expression of transcription factors KLF2 and KLF4.[36,42] In addition, disruption of endothelial apical-basal

polarity[50] and endothelial-to-mesenchymal transition, where stable endothelium of the blood vessels shift to possess stem-like characteristics, have been implicated in the pathophysiology of CCM.[51]

1.6. **KLF2 and KLF4 regulate gene expression in cerebral cavernous malformations**

The upregulation of KLF2 and KLF4 has been recognized to be an important hallmark and biomarker of CCMs.[41,52,53] Our group has recently performed a genome-wide transcriptome analysis of murine brain microvascular endothelial cells (BMEC) following time-controlled genetic inactivation of *Krit1* or *Pdcd10* in order to elucidate the pathogenesis of CCM **(Figure 4)**.[36,54] An important finding was upregulation in KLF2 and KLF4, confirming previous reports in murine endothelium and zebrafish endocardium.[41,52,53] Upregulation of endothelial KLF2 and KLF4 contributes to CCM formation, in part, by silencing TSP1 expression thereby contributing to an increased angiogenic phenotype and to abnormal vascular development.[36] Moreover, increased expression of KLF2 and KLF4 leads to upregulation of thrombomodulin (*Thbd*, which encodes TM) that in part can contribute to formation of an anticoagulant vascular domain that predisposes the CCM lesions to hemorrhages.[33]

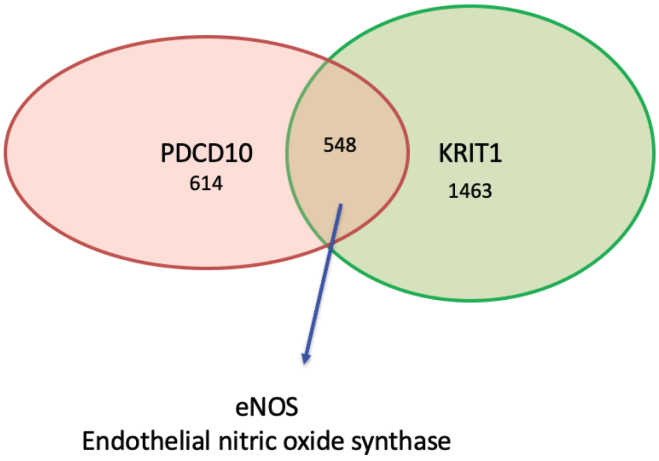

Figure 4. CCM Genome-Wide Transcriptome Analysis. Genome-wide RNA sequencing data from brain microvascular endothelial cells with inactivated *Krit1* or *Pdcd10* genes.

1.7. Objectives of the present study

Based on the transcriptome analysis, we selected *Nos3*, which encodes endothelial nitric oxide synthase (eNOS), for further investigation based on the following criteria: 1) *Nos3* was upregulated in both CCM3 (PDCD10) and CCM1 (KRIT1); 2) *Nos3* was among the highest upregulated factors; 3) eNOS can promote angiogenesis and vascular permeability, well known features of CCM; and 4) nitric oxide (NO) derived from eNOS can affect both the endothelium and perivascular astrocytes.

Here, I investigated the upregulation of eNOS and NO release observed following loss of brain endothelial PDCD10. eNOS expression results in increased production and secretion of NO, an important intercellular messenger in the CNS that has been implicated in molecular and cellular processes that lead to angiogenesis and vascular permeability.[10,36,55] In particular, NO has been implicated in the upregulation of VEGF,[56] a factor that has been associated with CCMs.[36,45,46,57]

Hence, the aims of the present work are:

1) To establish an *in vitro* CCM model by genetic inactivation of *Pdcd10* (*Pdcd10*^{ECKO}) BMECs in a time-controlled manner and determine changes in eNOS expression and NO release.
2) To establish the isolation and culture of mouse primary astrocytes and determine astrocyte-derived VEGF production in response to exogenous NO.
3) To investigate whether upregulation of eNOS expression and subsequent NO release in *Pdcd10*^{ECKO} BMECs induces astrocyte-derived VEGF by performing co-culture studies.
4) Based on novel findings observed in the previous aim, to further investigate the molecular mechanisms involved in astrocyte-induced exacerbation of CCMs.

2. Materials and Methods

2.1. Genetically modified mice

Endothelial-specific conditional *Pdcd10*-null mice were generated by crossing a *Pdgfb* promoter-driven tamoxifen-regulated Cre recombinase (*iCreERT2*)[58] with loxP-flanked *Pdcd10* (*Pdcd10*$^{fl/fl}$; generous gift from Wang Min, Yale University; *Pdgfb-iCreERT2;Pdcd10*$^{fl/fl}$) mice. eNOS-deficient mice (*Nos3*$^{-/-}$) were obtained from Jackson Laboratory and crossed with *Pdgfb-iCreERT2;Pdcd10*$^{fl/fl}$ mice to generate *Pdgfb-iCreERT2; Pdcd10*$^{fl/f}$*;Nos3*$^{-/-}$ and *Pdgfb-iCreERT2; Pdcd10*$^{fl/f}$*;Nos*$^{+/-}$ mice. On postnatal day 1, 2, and 3, mice were administered 50 μg of tamoxifen [T5648; Sigma-Aldrich] by intragastric injection to induce genetic inactivation of the endothelial *Pdcd10* gene in littermates with *iCreERT2* (*Pdcd10*^{ECKO}), and *Pdcd10*$^{fl/fl}$ mice were used as littermate controls. On postnatal day 1, 2, and 3, mice were administered 50 μg of tamoxifen [T5648; Sigma-Aldrich] by intragastric injection to induce genetic inactivation of endothelial *Pdcd10* gene in littermates with *iCreERT2; Nos*$^{+/-}$ or *iCreERT2; Nos*$^{-/-}$ (*Pdcd10*^{ECKO}*;Nos*$^{+/-}$ and *Pdcd10*^{ECKO}*;Nos*$^{-/-}$) and *Pdcd10*$^{fl/fl}$*;Nos*$^{+/-}$ or *Pdcd10*$^{fl/fl}$*;Nos*$^{-/-}$ mice were used as littermate controls, respectively. *Vegfa*$^{tm1.1Nagy}$ mice, expressing a B-galactosidase (LacZ) reporter gene inserted into the 3' untranslated region of the *Vegfa* gene, were obtained from the Jackson Laboratory.

2.2. Isolation of primary astrocytes

Vegfa$^{tm1.1Nagy}$ mice at postnatal day 5-7 were sacrificed, and their brains were isolated and placed into cold solution A (0.5% bovine serum albumin (BSA) in DMEM and 1 μg/μl glucose, 10mM HEPES, 1x penicillin-streptomycin). Brain cortices were separated from the brain and rolled on dry filter paper to detach and remove the meninges. Cortices from 8-11 mice were pooled and minced with scissors in solution A, and the tissue was centrifuged at 215g for 5 minutes at

4°C. The tissue pellet was digested with a papain solution (0.7mg/ml papain suspension [LS003126; Worthington], 20units/ml DNase I [11284932001; Sigma-Aldrich], and 0.150µg/ml tosyl-lysine-chloromethyl-ketone [T7254; Sigma-Aldrich]) at 37°C for 25 min with vigorous shaking every 10min. The tissue suspension was triturated using thin-tipped Pasteur pipettes until partially homogenous and centrifuged at 215g for 5 minutes. The pellet was resuspended with solution B (25% BSA in DMEM and 1µg/µl glucose, 10mM HEPES, 1x penicillin-streptomycin) and centrifuged at 1000g for 20min at 4°C. The lighter phase containing astrocytes was extracted, resuspended in 50ml of solution C (DMEM-1µg/µl glucose, 10mM HEPES, 1x penicillin-streptomycin), and centrifuged at 215g for 10 minutes at 4°C. The pellet was resuspended again in 50 ml of solution C and centrifugation was repeated.

2.3. Astrocyte culture conditions

The purified primary astrocytes were plated on a Poly-L lysine-coated plate (2.4 Growth surface preparation) cultured in astrocyte media comprised of 1:1 Neurobasal media and DMEM (1µg/µl glucose) supplemented with the following: 0.1mg/ml BSA, 0.1 mg/ml transferrin, 0.016mg/ml putrescine, 0.025µg/ml progesterone, 0.016µg/ml sodium selenite, 5ng/ml H-BEGF, 5µg/ml N-acetyl cysteine, 1mM sodium pyruvate, 1x penicillin-streptomycin, and 292µg/ml L-glutamine. The primary astrocyte culture identity and purity were confirmed by GFAP and integrin β5 immunofluorescence **(Figure 10)**.

2.4. Growth surface preparation

Poly-L lysine (P8920-100ml, 0.1% (w/v) in H20, Sigma-Aldrich) stock solution was diluted 1 in 10 in Hank's balanced salts solution plus calcium (HBSS+Ca) (14025092, Sigma-Aldrich) and left for 1h at 37°C on the plastic surface of 6-well plate format. Collagen type I

(C8919, 0.1% (w/v) in 0.1 M acetic acid) stock solution was diluted 1 in 20 in HBSS+Ca and left for 1h at room temperature (RT) on the plastic surface of 6-well plate format. For experiments that used transwell polyester membrane inserts (0.4 μm pore, CLS3450 24mm or CLS3460 12mm diameter, Corning Costar), the filters were first coated with Poly-L lysine as described. Coating solutions were removed, and cells were seeded onto the plastic surface or inserts.

2.5. Isolation of primary brain microvasculature endothelial cells

Adult mice 2-4 months old were sacrificed, and brains were isolated and placed into cold solution A. Meninges and choroid plexus were detached and removed, and the brains of 5-6 mice were pooled together and minced with scissors in solution A (2.2 Isolation of Astrocytes). Brain tissue suspension was centrifuged at 215g for 5 minutes at 4°C. The tissue was digested with a collagenase/dispase solution (1mg/ml collagenase/dispase [10269638001; Sigma-Aldrich], 20 units/ml DNase I [11284932001; Sigma-Aldrich], and 0.150μg/ml tosyl-lysine-chloromethyl-ketone [T7254; Sigma-Aldrich] in DMEM]) at 37°C for 1h with vigorous shaking every 10min. Then the tissue suspension was triturated using thin-tipped Pasteur pipettes until fully homogenous and centrifuged at 215g for 5 minutes. The pellet was resuspended in cold solution B (2.2 Isolation of Astrocytes) and centrifuged at 1000g for 20min at 4°C. The lighter phase was discarded and the heavy phase containing the brain microvasculature was digested in collagenase/dispase a second time for 30min at 37°C with vigorous shaking every 10min. After incubation, the suspension was centrifuged (215g for 5min at 4°C) and the pellet was resuspended in BMEC-media that comprised of EBM-2 medium (Lonza) supplemented with the following: 0.025% recombinant human EGF, 0.1% insulin-like growth factor, 0.1% gentamicin, 0.04% ascorbic acid, 0.04% hydrocortisone, and 20% FBS. The BMECs were plated in collagen-coated wells (0.005% collagen in HBSS

[C8919, Sigma-Aldrich]) and cultured in 10μg/ml of puromycin for 2 days, followed by 2μg/ml for 2 days. Primary BMEC culture identity and purity were confirmed by RNA expression levels of endothelial-specific genes, morphology, and immunofluorescence.

2.6. Inactivation of *Krit1* or *Pdcd10* gene in primary BMECs

After 5 days in culture at 37°C in 95% air and 5% CO_2, primary BMEC (2.5 Isolation of primary brain microvasculature endothelial cells) from mice bearing *Pdcd10*$^{fl/fl}$ or *Pdgfb-iCreERT2*;*Pdcd10*$^{fl/fl}$ (2.1 Genetically modified mice) were passaged to equal confluency (~ 2.5 x 10^5 cells) on collagen-coated 6-well plates. On day 6-7 from initial culture, *Pdgfb-iCreERT2*;*Pdcd10*$^{fl/fl}$ BMECs were treated with 5μM of 4-hydroxy-tamoxifen (H7904; Sigma-Aldrich) for 48h to delete *Pdcd10 (Pdcd10*^{ECKO}*). Pdcd10*$^{fl/fl}$ BMECs were also treated with 4-hydroxy-tamoxifen and used as a control. The deletion of *Pdcd10* in *Pdcd10*^{ECKO} BMECs was verified by RT-qPCR analysis **(Figure 5A)**. The medium was replaced with fresh BMEC-media (2.5 Isolation of primary brain microvasculature endothelial cells) and changed again every two days.

2.7. Co-culture of BMECs and astrocytes

Pdcd10^{ECKO} and *Pdcd10*$^{fl/fl}$ BMECs at passage 1-3 were plated on collagen-coated 6-well plates (2.5 Isolation of primary brain microvasculature endothelial cells and 2.6 Inactivation of *Krit1* or *Pdcd10* gene in primary BMECs) and maintained in BMEC-media for 15-20 days, while mouse primary astrocytes (~3.5 x 10^5 cells) were seeded on poly-L-lysine coated transwell filters (3450; Sigma-Aldrich) and maintained in astrocyte-media (2.3 Astrocyte culture conditions). Astrocytes were maintained for 3 days before transwells were placed onto the BMEC wells

containing astrocyte media supplemented with 500μM L-arginine. BMEC and astrocytes were maintained in co-culture for the time indicated in each experiment.

2.8. Immunofluorescence microscopy

Astrocytes were grown on poly-L-lysine coated 12-well transwell filters (CLS3460; Sigma-Aldrich) or cover glasses (12-545-81; Thermo Fischer Scientific) (2.3 Astrocyte culture conditions and 2.4 Growth surface preparation). For β-gal staining, cells were fixed for 5min at RT in a β-gal fixation solution (5mM EGTA, 2.5mM $MgCl_2$, 0.2% Glutaraldehyde, 1.3% PFA in PBS) and washed for 5 min at RT with β-gal washing buffer (2mM $MgCl_2$, 0.02% NP-40 in PBS). A β-gal staining was performed at 37°C for 3h in 0.02% X-Gal, 5mM $K_3Fe(CN)_6$, 5mM $K_4Fe(CN)_6$, 2mM $MgCl_2$ in PBS. After staining, astrocytes were fixed again with 4% PFA for 10 min at RT, pH 7.4, and permeabilized with 0.5% Triton X-100 in PBS for 5min. For astrocytes not undergoing β-gal staining, the cells were fixed for 10 min at RT with 4% PFA in PBS, pH 7.4, and permeabilized with 0.5% Triton X-100 in PBS for 5 min. The cells were blocked with 0.5% BSA for 30min and incubated with rat polyclonal antibodies anti-GFAP (1:80; 13-0300; Thermo Fischer Scientific), sheep polyclonal antibodies anti-ITβ5 (1:40, R&D Systems), and rabbit polyclonal antibodies anti-HIF-1α (1:150; NB100-134; Novus Biologicals) overnight at RT. Cells were washed four times with PBS and incubated with anti-rabbit Alexa Fluor 594 and anti-rat Alexa Fluor 488 secondary antibody (1:300, Thermo Fischer Scientific) in PBS for 1h at RT. Astrocyte nuclei were stained with DAPI and mounted with Fluoromount-G mounting medium (SouthernBiotech).

2.9. Immunohistochemistry

Brains from *Pdcd10*^{ECKO} and littermate control *Pdcd10*$^{fl/fl}$ mice at postnatal day 10 were isolated and fixed in 4% PFA at 4°C overnight. After cryoprotection in 30% sucrose dissolved in PBS, brains were embedded and frozen in O.C.T compound (23-730-571; Fischer Scientific). Cerebellar tissues were cut into 12-µm coronal sections onto Superfrost Plus slides (12-550-15; VWE International). Sections were blocked and permeabilized in a permeabilization solution (0.5% Triton X-100, 5% goat serum, 0.5% BSA, in PBS) for 2h and incubated in rabbit polyclonal antibodies against eNOS (1:200; PA1-037; Thermo Scientific) in PBS at room temperature overnight. Preparations were washed one time in brain-Pblec buffer (PBS, 1mM $CaCl_2$, 1mM $MgCl_2$, 0.1 mM $MnCl_2$, and 0.1% Triton X-100) and incubated with isolectin B4 FITC conjugated (1:80, L2895; Sigma-Aldrich) in Pblec buffer at 4C overnight. Tissue sections were washed four times in PBS and incubated with suitable anti-rabbit Alexa Fluor 594-coupled secondary antibody (1:300, Thermo Fischer Scientific) in PBS for 1h at RT. Cell nuclei were stained with DAPI and mounted with Fluoromount-G mounting medium (SouthernBiotech).

2.10. Western blot analysis

BMECs were lysed using a solution containing 1mM sodium orthovanadate, protease inhibitor cocktail (11836170001; Roche), and 100µL of radioimmunoprecipitation assay buffer (Thermo Scientific). A Micro BCA protein assay kit (500-0116; Thermo Scientific) was used to determine the protein concentration and 25µg of cell lysates were heated for 5 minutes at 95°C to denature all proteins. The cell lysates were subjected to a 4% to 20% gradient sodium dodecyl sulfate-polyacrylamide gel electrophoresis (XP04200, Thermo Fischer Scientific) and a wet transfer was used to transfer proteins to nitrocellulose membranes (Amersham). Membranes were

blocked for 1h at RT using a blocking solution (TBS 1x, 10% nonfat milk), and polyclonal rabbit antibodies directed against eNOS (1:500; PA1-037; Thermo Scientific) or HIF-1α (1:150; NB100-134; Novus Biologicals) were incubated at 4°C overnight. Several washes were performed and then the membranes were incubated with appropriate IRDye/Alexa Fluor-coupled secondary antibodies (1:10,000, 926-68070; 926-32211; Li-COR) for 1h at RT. A mouse monoclonal antibody against beta-actin (1:5000; A5441; Sigma-Aldrich) was used as a control for protein loading. Membranes were imaged and analyzed using Odyssey CLx Infrared Imaging (Li-COR).

Lysis solution: radioimmunoprecipitation assay (RIPA) buffer [25mM Tris/HCl pH 7.6, 150mM NaCl, 0.1% sodium dodecyl sulfate (SDS), 1% NP-40, 1% sodium deoxycholate], protease inhibitor cocktail (11836170001, Roche), and 1mM sodium orthovanadate.

Laemmli's sample buffer 4 X: 0.01% bromophenol blue, 40% glycerol, 8% SDS, 15mg/ml D,L-dithiothreitol, in 250mM Tris/HCl pH 6.8

Running buffer: 125mM Trizma base, 1M glycine, and 0.01% (v/v) SDS in ddH_2O prepared from 10X stock.

Transfer buffer: 50mM Trizma base, 40mM, 20% (v/v) methanol in ddH_2O

Blocking buffer: 0.1% tween-20, 10% fat-free dried milk dissolved in TBS at pH 7.4.

Washing buffer: 0.1% tween-20 dissolved in TBS at pH 7.4.

Molecular weight marker: Precision Plus Protein dual color standard (1610374, BioRad).

2.11. RNA isolation

Total RNA from cultured astrocytes and BMECs (2.2 Isolation of primary astrocytes and 2.5 Isolation of primary brain microvascular endothelial cells) were isolated by TRIzole as

specified by the manufacturer's protocol (Thermo Fischer Scientific). Briefly, 1ml of TRIzole reagent was added per well. Cell homogenization was completed by pipetting up and down several times throughout the entire surface area where cells were growing. Cell lysates were transferred to Phase Lock Gel 2ml tubes (2302830; VWR). Then, 200µl of chloroform (ICN19400290; Thermo Fischer Scientific) was added to each tube and mixed vigorously for 15 seconds, followed by a 3-minute incubation at room temperature prior to centrifugation at 12,000g for 15 minutes at 4°C. The aqueous phase containing RNA was collected and transferred to a 1.5ml DNAse/RNAse free microfuge tube. To precipitate the RNA, 500µl of isopropanol was added, resuspended, and incubated for 10 minutes at room temperature followed by centrifugation at 12,000g for 10 minutes at 4°C. The supernatant was removed, and the pellet was washed with 1ml of 75% ethanol followed by centrifugation at 7,500g for 5 minutes at 4°C. The supernatant was removed, and the pellet was air-dried at room temperature and dissolved in 11µl-20µl of DNAse/RNAse free water. To determine the concentration and purity, 1µl of each sample was analyzed using UV spectrophotometry at 260 and 280 nm using NanoDrop 1000 Spectrophotometer.

2.12. RT^2-qPCR analysis

10ng of total RNA was used to produce single-stranded complementary DNA (cDNA) using random primers according to the manufacturer's protocol (48190011; 18080093; Thermo Fischer Scientific). Briefly, 10ng of RNA was added to a master mix containing 1X First-Strand buffer, 1µl 0.1M DTT, 1mM dNTPs, 1µl RNaseOUT recombinant RNase inhibitor, SuperScript III reverse transcriptase, and 0.5µg random primers. The mixture was placed in a thermal cycler (C1000 Touch, Bio-Rad) at 25°C for 10 minutes, and then incubated at 50°C for 1 hour followed by inactivation of the reaction by heating at 70°C for 15 minutes. 300ng of cDNA was run with

the Kapa SybrFast qPCR mix (Kapa Biosystems) using 50μM of primers to distinguish between the relative levels of genes in each condition. The PCR reaction was placed in a thermal cycler (C1000 Touch, Bio-Rad) using an initial step at 95°C for 15 minutes, followed by 40 cycles (30sec at 95°C, 30sec at 55°C, and 30sec at 72°C). Analysis of the data was performed using the $2^{-\Delta\Delta CT}$ method,[56] and the relative quantification was determined as follows:

Threshold cycle (C_T) values were determined by the cycle number at which the fluorescence curve crosses a predetermined threshold, usually 10 to 50 times the standard deviation of baseline fluorescence. The threshold for each experiment was assigned to be within the linear phase of the amplification curve. Differences in C_T between target genes (i.e. *Pdcd10, Nos3*) and the internal control (*Actin*) was calculated using the following formula:

$$\Delta C_T = C_T \text{ target} - C_T \text{ internal control}$$

The difference in ΔC_T between each condition and that of the appropriate control or vehicle ($\Delta\Delta C_T$) was calculated using the following formula:

$$\Delta\Delta C_T = \Delta C_T \text{ condition} - \Delta C_T \text{ control}$$

Relative levels of mRNA were normalized to those measured in control samples, and then transformed into absolute values using the following formula:

$$\text{Comparative mRNA expression levels} = 2^{-\Delta\Delta CT}$$

2.13. NO Determination

Pdcd10^{ECKO} and *Pdcd10*$^{fl/fl}$ BMECs (2.6 Inactivation of *Pdcd10* gene in primary BMECs) were maintained in BMEC media supplemented with 500μM L-Arginine and deficient in fetal bovine serum and ascorbic acid for 36 hours. Then, the BMEC media was collected, and a

colorimetric total nitric oxide assay was performed as specified by manufacturers protocol (KGE001; R&D Systems). 50µl of undiluted BMEC media samples and nitrate (NO_3) standards ranging 100µM to 1.565µM were plated on clear polystyrene microplates (DY990; R&D Systems). To measure total nitrites (NO_2) and nitrates, 25µl of nitrate reductase and 25µl of NADH were added to each well to convert all available nitrates to nitrite. The plate was covered with an adhesive strip and incubated at 37°C for 30 minutes. After incubation, 50µl of Griess reagent I and Griess reagent II were added to all wells and incubated at room temperature for 10 minutes. A two-step diazotization reaction occurs in which NO_2^- reacts with sufanilic acid to produce a diazonium ion, which is then coupled to N-(1-naphthyl) ethylenediamine to form an azo-derivative that absorbs light at 540nm. The optical density (O.D.) of each well was read using a microplate reader (Infinite 200 PRO, Tecan) at 540nm with a wavelength correction of 690nm. Duplicate readings were averaged and normalized to the blank. A standard curve was generated for each experiment by plotting optical density against concentration (µM), and total nitrate/nitrite concentrations were determined using the linear trendline.

2.14. Statistics

Statistical analysis for single comparisons was performed using a two-tailed student's *t*-test and analysis for multiple comparisons was performed using ANOVA followed by a Bonferroni post hoc test. The threshold for statistical significance was set at a *p*-value of 0.05.

Chapter 2, in part, is currently being prepared for submission for publication of the material. Soliman, Shady; Hale, Preston; Pham, Angela; Lai, Catherine; Lagarrigue, Frederic; Sun, Hao; Ginsberg, Mark H. and Lopez-Ramirez, Miguel A. The thesis author is a coauthor of this material.

3. Results

3.1. Brain endothelial genetic inactivation of *Pdcd10* (CCM3) increases eNOS expression

Recently, our lab performed a genome-wide transcriptome analysis of cultured BMECs after genetic inactivation of *Pdcd10* (*Pdcd10*^{ECKO}) or *Krit1* (*Krit1*^{ECKO}) and identified increased *Nos3* mRNA levels.[36,54] To validate that finding, we repeated experiments by isolating BMECs from mice carrying floxed alleles in the *Pdcd10* (*Pdcd10*$^{fl/fl}$) gene in the presence or absence of a Cre-recombinase gene under the control of an endothelial-specific promoter (*Pdgfb-iCreERT2*).[58] Treatment of *Pdgfb-iCreERT2*;*Pdcd10*$^{fl/fl}$ BMECs with 4-hydroxy-tamoxifen deleted *Pdcd10* (*Pdcd10*^{ECKO}) and reduced *Pdcd10* mRNA by ~98.2% within 9 days compared with 4-hydroxy-tamoxifen treated *Pdcd10*$^{fl/fl}$ BMECs **(Figure 5A)**. We observed by RT-qPCR analysis that upregulation of *Nos3* mRNA (~19.2 fold increase) was associated with increased eNOS protein expression (~8.9 fold increase) in *Pdcd10*^{ECKO} BMECs when compared to *Pdcd10*$^{fl/fl}$ BMEC control as assessed by Western blot analysis **(Figure 5B,C)**. These results indicate that upon genetic inactivation of *Pdcd10* in BMECs, there is a significant increase in eNOS mRNA and protein levels.

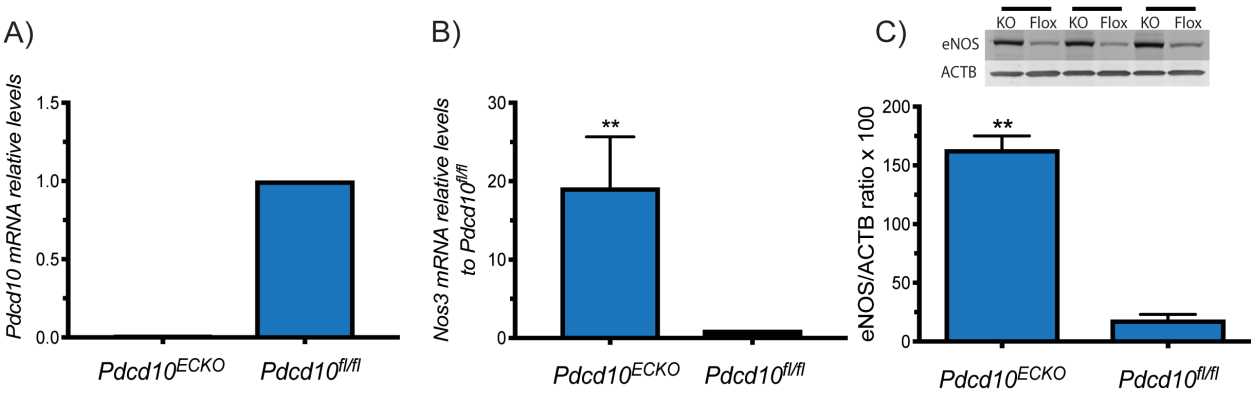

Figure 5. Inactivation of *Pdcd10* in BMECs increases eNOS expression. A) RT-qPCR analysis of *Pdcd10* mRNA levels from inactivated *Pdcd10*^{ECKO} BMECs compared to *Pdcd10*$^{fl/fl}$ BMECs (control) (SEM, n = 3). B) RT-qPCR analysis *of Nos3* mRNA in *Pdcd10*^{ECKO} BMECs compared to *Pdcd10*$^{fl/fl}$ BMECs (control) (SEM, n = 3). C) Quantification of eNOS protein from *Pdcd10*^{ECKO} BMECs compared to *Pdcd10*$^{fl/fl}$ BMECs (SEM, n = 3). Student's t-test, ** $P < 0.01$.

3.2. Loss of brain endothelial *Pdcd10* increases the expression of eNOS *in situ*

To determine if the loss of endothelial *Pdcd10* also induced increased expression of eNOS mRNA and protein *in situ,* we analyzed the hindbrains of $Pdcd10^{ECKO}$ or $Pdcd10^{fl/fl}$ mice and performed analysis by RT-qPCR, Western blot, and immunofluorescence. At P9, $Pdcd10^{ECKO}$ hindbrains show notable vascular lesions when compared with littermate $Pdcd10^{fl/fl}$ controls **(Figure 6)**.

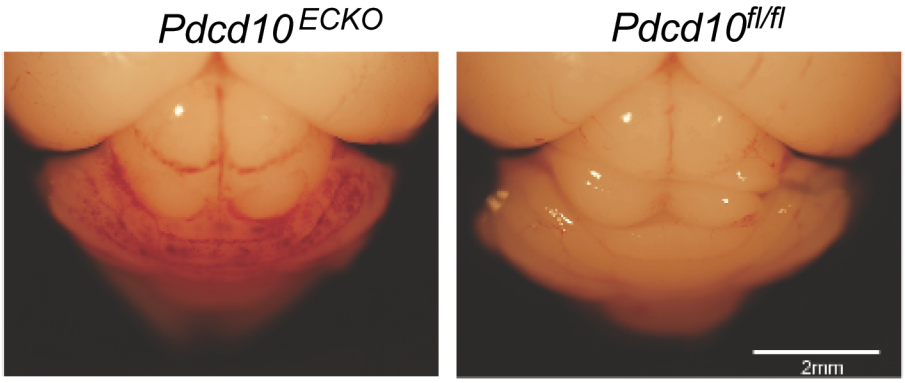

Figure 6. Inactivation of endothelial *Pdcd10* induces CCM lesions in mouse hindbrains. 50 μg of tamoxifen was injected intragastrically on postnatal days 1,2, and 3. At P9, the brains were isolated, and the cerebellum was analyzed. Scale bar, 2mm.

Consistent with results observed in cultured experiments, $Pdcd10^{ECKO}$ hindbrains showed ~3.3 fold increase in *Nos3* mRNA levels compared with littermates $Pdcd10^{fl/fl}$ control. Furthermore, Western blot analysis showed a ~5.8 fold increase in eNOS protein expression in $Pdcd10^{ECKO}$ hindbrains relative to $Pdcd10^{fl/fl}$ hindbrains **(Figure 7A,B)**. Analysis of hindbrain sections revealed that eNOS was upregulated in the CCM lesions. As showed in Figure 7C, we observed that eNOS staining was increased in $Pdcd10^{ECKO}$ vasculature as showed by colocalization of antibodies specific against eNOS and isolectin B4-FITC, which specifically labels the brain vasculature **(Figure 7C)**. Together these results demonstrate that eNOS mRNA and protein expression is increased as a result of the loss of endothelial *Pdcd10*.

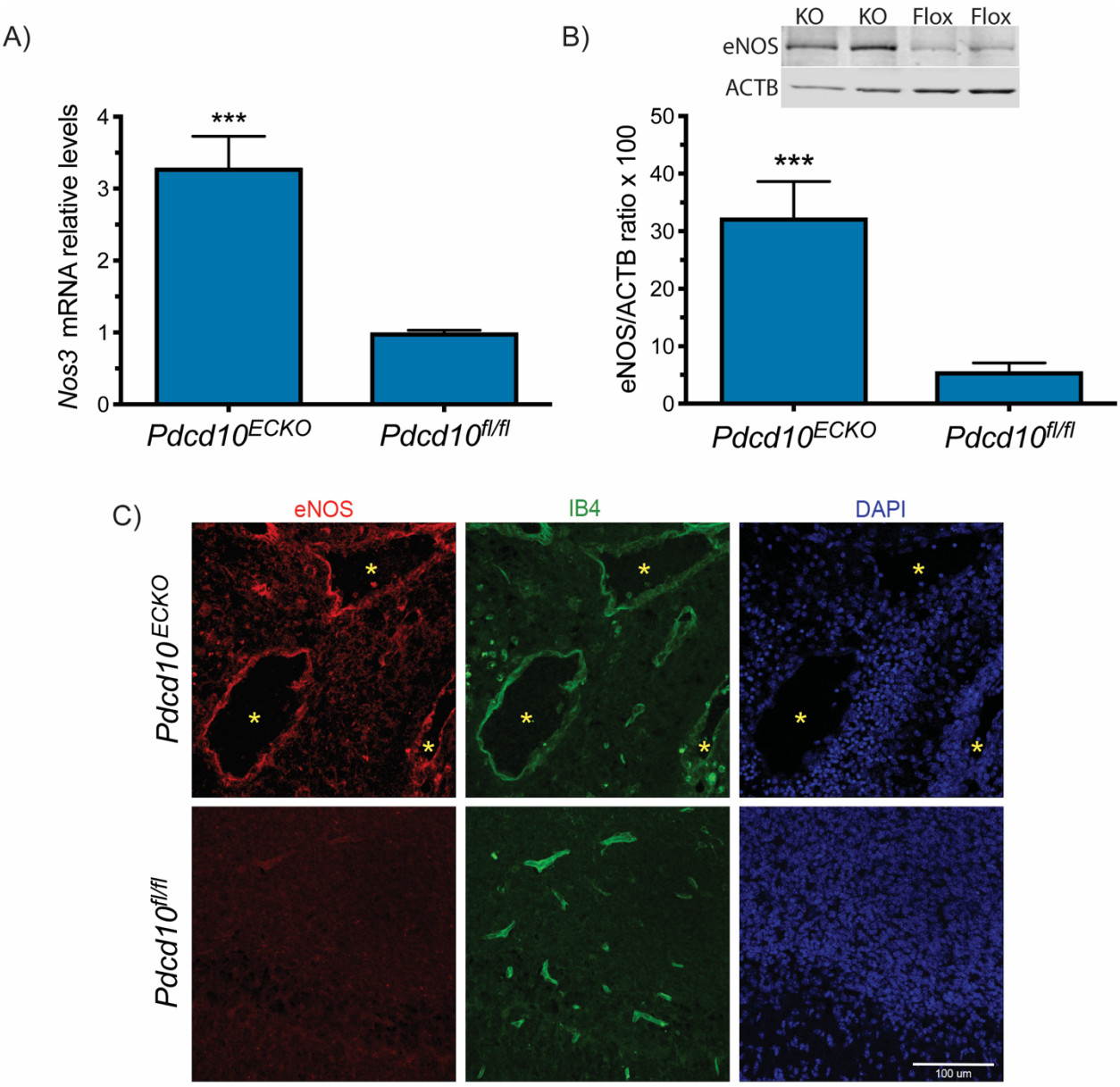

Figure 7. Loss of brain endothelial *Pdcd10* induces the expression of eNOS *in situ*. A) RT-qPCR analysis of *Nos3* mRNA in *Pdcd10*^{ECKO} hindbrains compared to *Pdcd10*$^{fl/fl}$ hindbrains. (SEM, n = 5). B) Quantification of eNOS protein from *Pdcd10*^{ECKO} hindbrains compared to *Pdcd10*$^{fl/fl}$ hindbrains (SEM, n = 4). C) Immunofluorescence staining of eNOS (red) and isolectin B4 (green) in cerebellar sections from *Pdcd10*^{ECKO} or *Pdcd10*$^{fl/fl}$ mice at P9. DAPI staining (blue) was used to reveal the nuclei of sections. Asterisks indicate the vascular lumen of CCM lesions. Scale bar, 100um. Student's t-test, *** $P < 0.001$.

3.3. Loss of brain endothelial *Pdcd10* increases nitric oxide production

Endothelial cells metabolize L-arginine via eNOS to produce nitric oxide (NO), therefore we next investigated if upregulation of eNOS led to elevated NO production in *Pdcd10*^{ECKO}

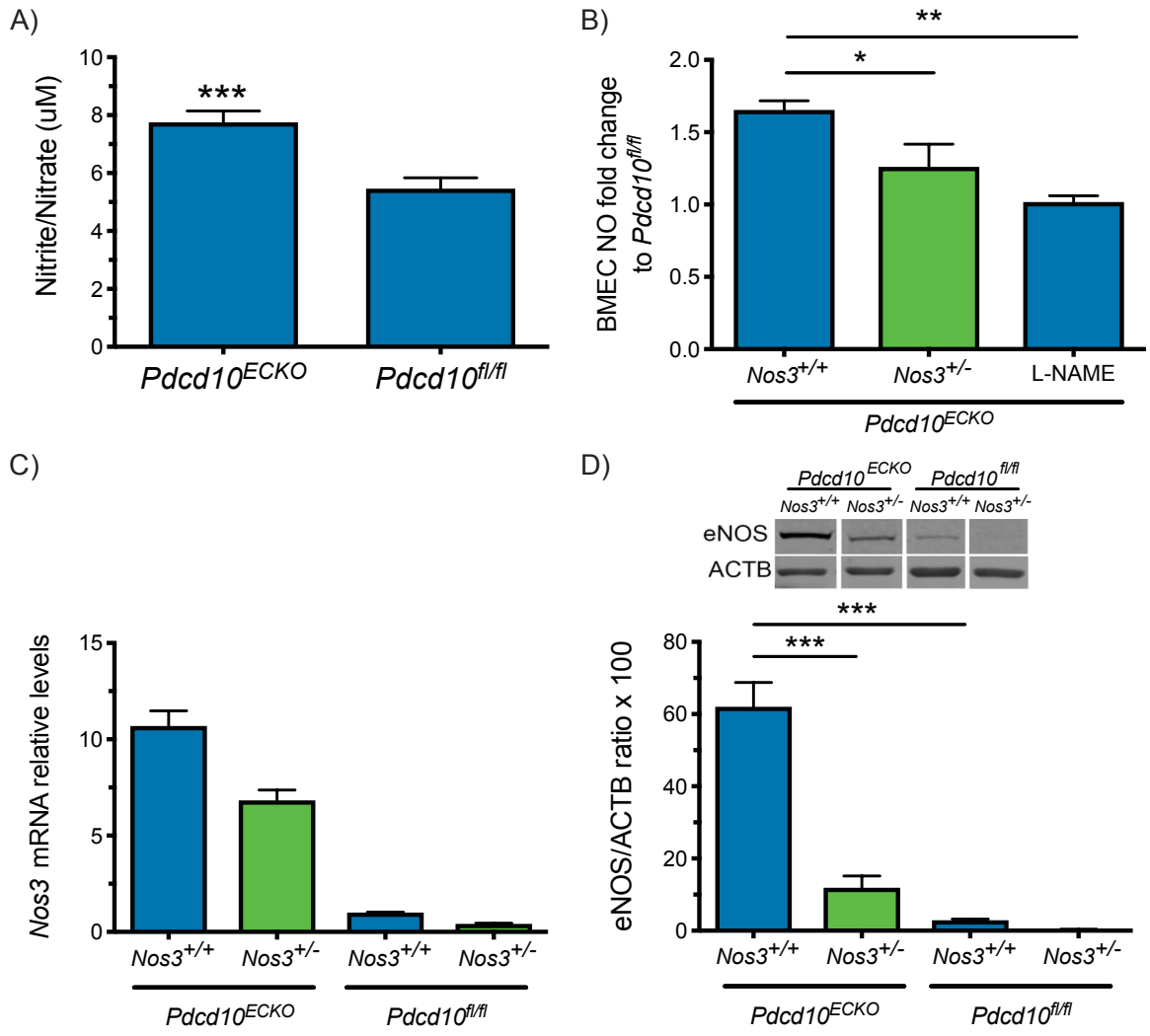

Figure 8. Loss of brain endothelial *Pdcd10* increases nitric oxide production. A) Total nitrite and nitrate concentration was determined by colorimetric assay analysis from the media of *Pdcd10*^{ECKO} and *Pdcd10*$^{fl/fl}$ BMECs that are *Nos3*$^{+/+}$cultured for 36hrs (SEM, n = 7). B) *Pdcd10*^{ECKO} and *Pdcd10*$^{fl/fl}$ BMECs that are *Nos3*$^{+/+}$ or *Nos3*$^{+/-}$ were compared to determine the fold change of total nitrites and nitrates in cultured media. The NOS inhibitor, L-NAME (150μM), was supplemented in culture media (n = 3). C) RT-qPCR analysis of *Nos3* mRNA levels in *Pdcd10*^{ECKO} *Nos3*$^{+/+}$ and *Pdcd10*^{ECKO} *Nos3*$^{+/-}$ BMECs relative to control (n = 2). D) Quantification of eNOS protein from *Pdcd10*^{ECKO} *Nos3*$^{+/+}$ and *Pdcd10*^{ECKO} *Nos3*$^{+/-}$ BMECs relative to control (n = 5). Culture media was supplemented with 500uM L-Arginine and was deficient in serum. Student's t-test, *P < 0.05, ** P < 0.01, *** P < 0.001.

BMEC. Using a colorimetric assay to quantitatively measure total NO_2 and NO_3 (nitrites and nitrates) in the culture media, we observed that *Pdcd10*^{ECKO} BMEC possessed a ~1.7 fold increase in NO release when compared with *Pdcd10*$^{fl/fl}$ BMEC control (NO basal levels: 5.47μM) **(Figure 8A)**. This result is consistent with the increased *Nos3* mRNA and eNOS protein levels observed in *Pdcd10*^{ECKO} BMEC. The increase in NO release is ascribable in part to the upregulation of eNOS, because genetic inactivation in one copy of the *Nos3* gene (*Nos3*$^{+/-}$) significantly reduced NO production in *Pdcd10*^{ECKO} BMEC **(Figure 8B)**. Consistent with these results, low levels of *Nos3* mRNA and eNOS protein in *Pdcd10*^{ECKO}*;Nos3*$^{+/-}$ BMEC were observed **(Figure 8C,D)**. Moreover, addition of a nitric oxide synthase (NOS) inhibitor, L-NAME, reduced NO production **(Figure 8B)** without changing eNOS mRNA and protein levels (data not shown). Taken together, these studies show that the loss of *Pdcd10* in BMECs lead to an increase in eNOS expression and subsequent endothelial NO release.

3.4. Astrocytes support CCM lesion formation

Postnatal hindbrain sections of *Pdcd0*^{ECKO} mice were labeled with anti-CD34 antibodies to label the vasculature and anti-GFAP antibodies to label astrocytes. Grossly-dilated blood vessels were observed in *Pdcd10*^{ECKO} hindbrains when compared to *Pdcd10*$^{fl/fl}$ control sections that showed conserved vascular integrity. Strikingly, lesions occurred only in areas that were enriched with astrocytes and that were residing in regions of the white matter **(Figure 9)**. These observations suggested that astrocytes associated with the CCM lesions could be contributing to CCM onset and exacerbation.

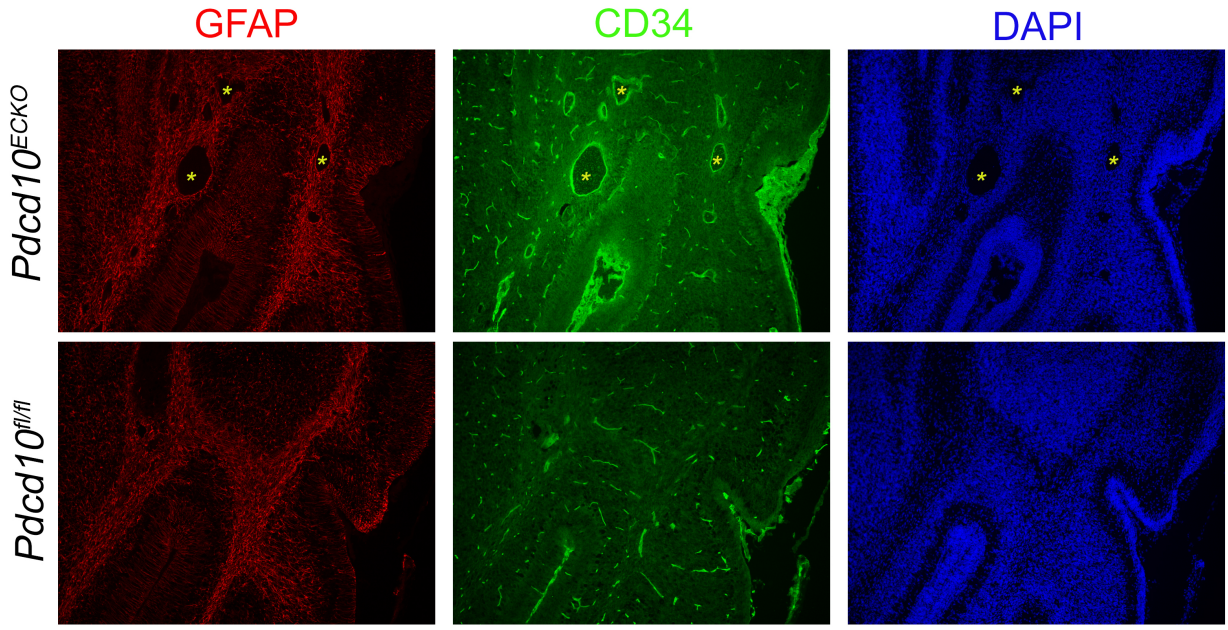

Figure 9. Astrocytes support CCM lesion formation. Immunofluorescence staining of GFAP (red) and CD34 (green) in cerebellar sections from *Pdcd10*^{ECKO} or *Pdcd10*$^{fl/fl}$ mice at P9. DAPI staining (blue) was used to reveal the nuclei of sections. Asterisks indicate the vascular lumen of CCM lesions.

3.5. Nitric oxide increases astrocyte-derived VEGF

Previously, it has been shown that NO donors, such as DETANONOate, increase angiogenesis by upregulation of VEGF in an animal model of ischemic stroke.[59] To investigate whether NO stimulates the expression of VEGF in astrocytes, we prepared primary mouse astrocyte cultures from VEGF-LacZ reporter mice (*Vegfa*$^{tm1.1Nagy}$), a reporter line that carries a nuclear-localized beta-galactosidase knock-in at the 3' UTR of the *Vegfa* gene locus that permits single-cell monitoring of VEGF expression.[60] We observed that the purity of cultured astrocytes was high as determined by cells that are double positive for specific astrocyte markers GFAP and integrin B5 **(Figure 10)**.

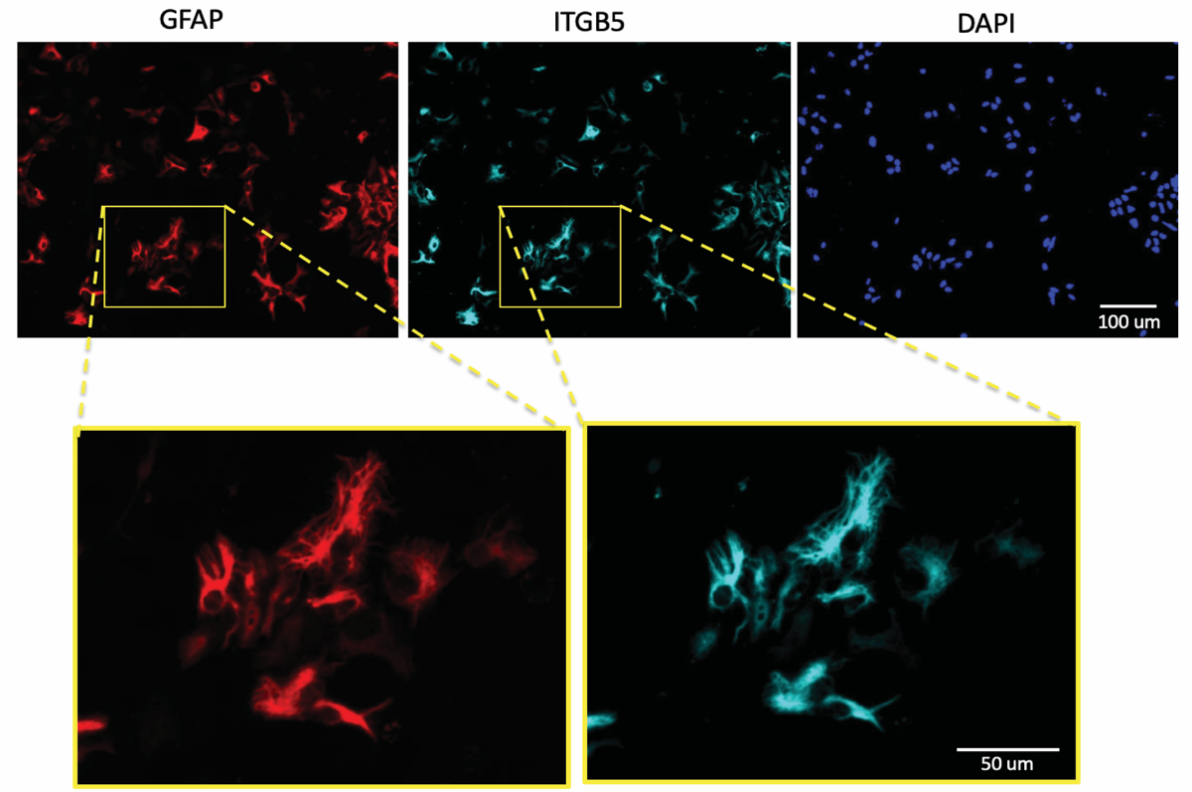

Figure 10. Primary cultured astrocytes. Immunofluorescence staining for GFAP (red) and integrin β5 (cyan) of primary cultured astrocytes from Vegfa$^{tm1.1Nagy}$ mice. Scale bar, 100μm, 50μm.

We observed that primary cultures of astrocytes (as shown by positive staining for GFAP) treated with 0.5mM DetaNONOate (NO donor) for 24h led to a dramatic increase in β-gal staining, an indicator of increased VEGF expression,[61] when compared with vehicle-treated astrocytes **(Figure 11A)**. We also observed that the effect of DETANONOate inducing increased β-gal staining can be prevented when astrocytes are pre-treated with 15μM CPTIO, a NO scavenger. Moreover, lower β-gal staining was observed in astrocytes pre-treated with only CPTIO when compared with control astrocytes **(Figure 11A)**. These results are consistent with our observations using RT-qPCR analysis. The addition of DETANONOate in astrocyte culture media induced a ~7 fold increase in astrocyte *Vegfa* and an ~11.50 fold increase in astrocyte *β-gal* mRNA levels **(Figure 11B)**, an effect that was prevented in astrocytes pre-treated with CPTIO **(Figure 11C)**.

These results indicate that our primary astrocyte cultures respond to exogenous NO and that elevated levels of NO can increase astrocyte-derived VEGF.

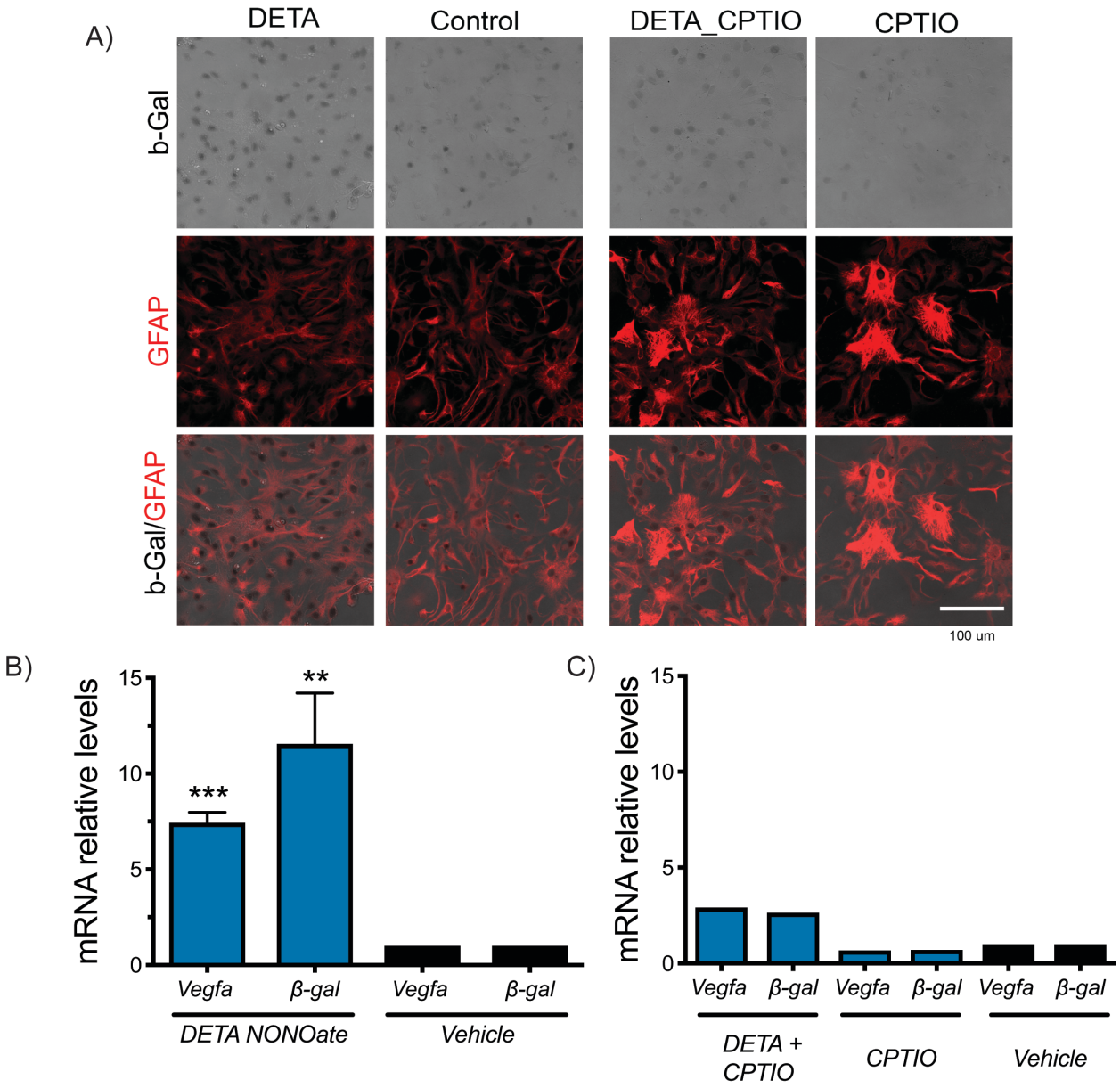

Figure 11. Nitric oxide induces astrocyte-derived VEGF. A) Immunofluorescence staining of GFAP (red) and β-gal staining of primary cultured astrocytes from Vegfa$^{tm1.1Nagy}$ mice cultured for 24 in with 0.5mM DETA NONOate and 15µM CPTIO. Scale bar, 100µm. B) RT-qPCR analysis of *Vegfa* and *β-gal* mRNA in primary cultured astrocytes treated with 0.5mM DETA NONOate for 24hrs. (SEM, n = 4). C) RT-qPCR analysis of *Vegfa* and *β-gal* mRNA in primary cultured astrocytes treated with 15µM CPTIO for 24hrs (n = 1). Student's t-test, ** $P < 0.01$, *** $P < 0.001$.

3.6. Brain endothelial nitric oxide induces astrocyte-derived VEGF following loss of *Pdcd10*

VEGF signaling is enhanced in CCM[57,62] and can contribute to the pathogenesis of CCM.[36] To investigate if brain endothelial NO induces astrocyte-derived VEGF during CCM, we co-cultured purified astrocytes and *Pdcd10*^{ECKO} or *Pdcd10*$^{fl/fl}$ BMECs in serum-free conditions supplemented with L-arginine and measured changes in the gene expression of the astrocytes. We observed that *Pdcd10*^{ECKO} BMEC significantly increase astrocyte-derived *Vegfa* mRNA levels **(Figure 12A)** in a co-culture system. In addition, using the bicistronic expression of *β-gal* as a *Vegfa* reporter, we also found that *β-gal* mRNA levels in astrocytes were significantly elevated when co-cultured with *Pdcd10*^{ECKO} BMEC compared to *Pdcd10*$^{fl/fl}$ BMEC control **(Figure 12B)**. Furthermore, we observed that the increase in astrocyte-derived *Vegfa* or *β-gal* mRNA levels was specific to the upregulation of eNOS, because genetic inactivation of one copy of the *Nos3* gene in *Pdcd10*^{ECKO} BMEC was sufficient to prevent *Vegfa or β-gal* upregulation in astrocytes **(Figure 12A,B)**. These data provide strong evidence that brain endothelial NO increases expression of astrocyte-derived VEGF following loss of endothelial *Pdcd10*.

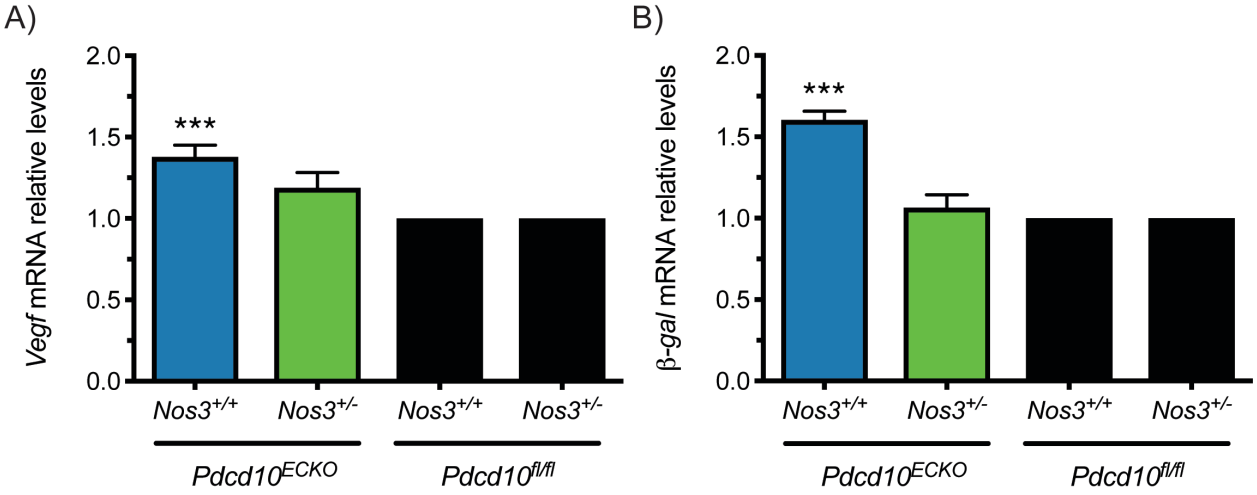

Figure 12. Brain endothelial NO induces astrocyte-derived VEGF following loss of *Pdcd10*. A) RT-qPCR analysis of *Vegfa* mRNA in primary cultured astrocytes co-cultured with *Pdcd10*^{ECKO} BMEC compared to *Pdcd10*$^{fl/fl}$ BMEC control (SEM, n = 4). B) RT-qPCR analysis of *β-gal* mRNA in primary cultured astrocytes co-cultured with *Pdcd10*^{ECKO} BMEC compared to *Pdcd10*$^{fl/fl}$ BMEC control (SEM, n = 4). Student's t-test, *** $P < 0.001$.

3.7. HIF-1α stabilization induces VEGF expression

Brain endothelial NO has been reported to stabilize hypoxia inducible factor 1 alpha (HIF-1α) in astrocytes and augment synthesis of VEGF in response to mild hypoxia.[63] Therefore, we next investigated whether brain endothelial NO induces astrocyte-derived VEGF expression by stabilizing HIF-1α following the loss of *Pdcd10*. For these studies, we co-cultured purified astrocytes and *Pdcd10*^{ECKO} or *Pdcd10*$^{fl/fl}$ BMECs in astrocyte serum-free conditions supplemented with L-arginine for 48h. Immunocytochemistry revealed elevated levels of HIF-1α in astrocytes co-cultured with *Pdcd10*^{ECKO} BMEC as compared with co-cultures in control *Pdcd10*$^{fl/fl}$ BMEC **(Figure 13A)**.

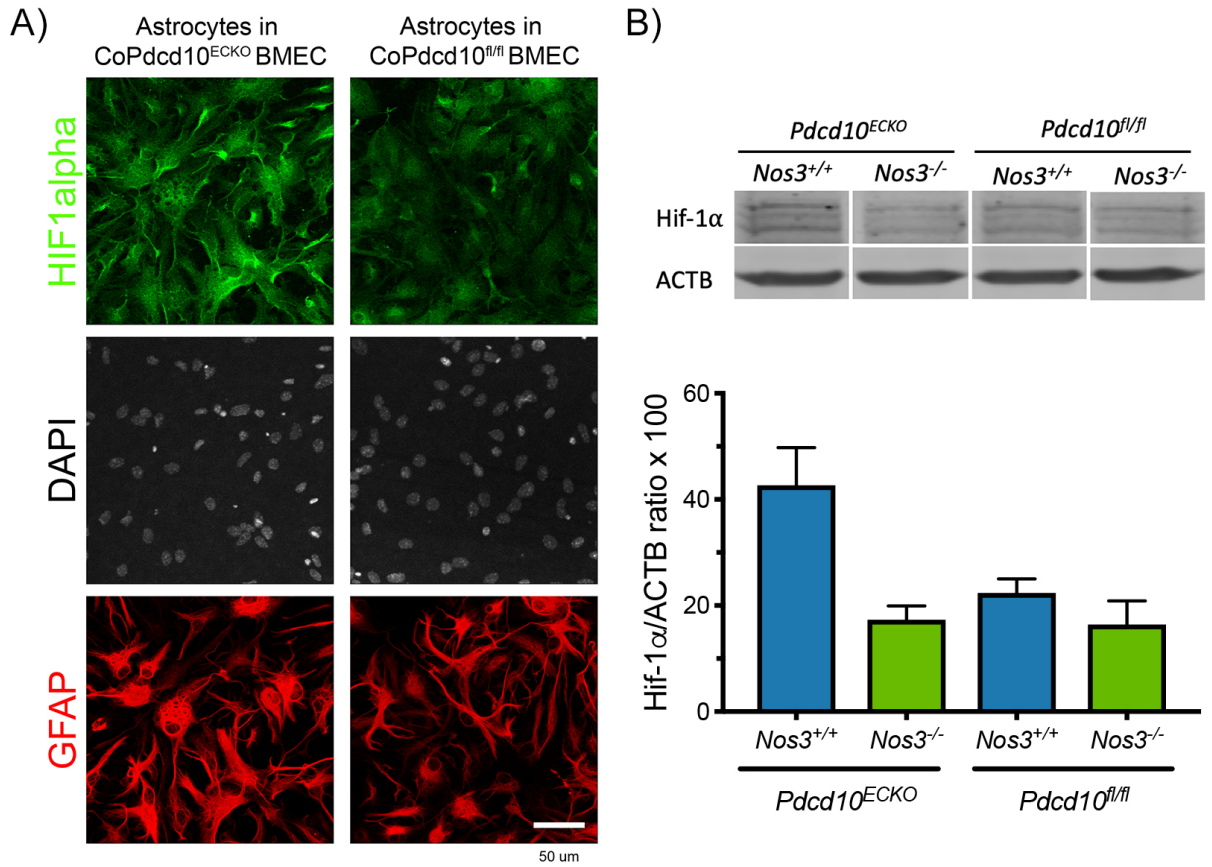

Figure 13. Brain endothelial NO stabilizes astrocyte HIF-1α following the loss of *Pdcd10*. A) Immunofluorescence staining for HIF-1α (green) and GFAP (red) of primary cultured astrocytes co-cultured with *Pdcd10*^{ECKO} BMEC compared to *Pdcd10*$^{fl/fl}$ BMEC control for 48hrs. Scale bar, 50μm. B) Quantification of HIF-1α protein from primary cultured astrocytes co-cultured with *Pdcd10*^{ECKO} BMEC compared to *Pdcd10*$^{fl/fl}$ BMEC control for 48hrs (SEM, n = 2).

Consistent with the observation of increased HIF-1α staining, western blot analysis confirmed an increase in HIF-1α protein levels in astrocytes co-cultured with *Pdcd10*^{ECKO} BMEC **(Figure 13B)**. The increase in HIF-1α protein was specific to the upregulation of eNOS, because genetic inactivation of both copies of the *Nos3* gene (*Nos3*$^{-/-}$) reduced HIF-1α protein stability in *Pdcd10*^{ECKO} BMEC **(Figure 13B).**

Chapter 3, in part, is currently being prepared for submission for publication of the material. Soliman, Shady; Hale, Preston; Pham, Angela; Lai, Catherine; Lagarrigue, Frederic; Sun, Hao; Ginsberg, Mark H. and Lopez-Ramirez, Miguel A. The thesis author is a coauthor of this material.

4. Discussion

CCMs are hypersensitive to angiogenesis due to the loss of an anti-angiogenic checkpoint[36] and increased VEGF signaling, leading to disassembly of brain endothelial tight junctions, dilation of vessels, and vascular leakage.[45,46] Here, we report that loss of PDCD10 in brain endothelial cells causes upregulation of eNOS mRNA and protein, as well as increased eNOS staining in CCM lesions. Furthermore, elevated eNOS levels results in an increased production and secretion of NO, an important intercellular messenger in the CNS responsible for vascular remodeling and angiogenesis.[59,64,65] To analyze the effect of upregulated eNOS and elevated release of NO during CCM, we prepared co-culture studies using purified astrocytes and *Pdcd10*^{ECKO} BMEC. Increased brain eNOS induced upregulation of astrocyte-derived *Vegfa.* The increase in astrocyte-derived *Vegfa* mRNA levels was specific to the upregulation of eNOS because genetic inactivation of one copy of the *Nos3* gene in *Pdcd10*^{ECKO} BMEC was sufficient to prevent *Vegfa* upregulation in astrocytes. Moreover, upregulation of eNOS in *Pdcd10*^{ECKO} BMEC was correlated to HIF-1α protein stabilization in astrocytes during co-culture studies, suggesting a NO-dependent HIF-1α stabilization. These studies identify that an increase in expression of eNOS during CCM may lead to a sustained increase in NO levels and induce astrocyte-derived VEGF production by HIF-1α protein stabilization. Therefore, we propose the possibility that CCM lesion formation and progression can be mediated by the non-cell-autonomous release of VEGF from perivascular astrocytes.

Elevated levels of endothelial-derived NO can induce non-cell-autonomous signaling during CCM. The diffusion of NO from endothelial cells to perivascular astrocytes increased astrocytic HIF-1α stabilization and subsequent synthesis of VEGF. At physiological levels of

oxygen, prolyl hydroxylases (PHDs) catalyze the iron-dependent hydroxylation of proline residues in HIF-1α (Pro-402 and Pro-564). As a result, von-Hippel-Lindau protein binds to HIF-1α and targets it for ubiquitin-dependent proteasomal degradation. Under hypoxic conditions, PHDs become inactivated, leading to HIF-1α stabilization. HIF-1α then translocates to the nucleus where it dimerizes with HIF-1β and binds to the hypoxia-responsive element in the promoter region of several target genes, including VEGF-A.[65–67] In addition to being regulated by oxygen, previous studies have demonstrated that high concentrations of NO can also stabilize the HIF-1α complex, rendering it active. Proposed mechanisms include the following: NO may bind to the iron co-factor of PHD and inhibit its ability to target HIF-1α for degradation; NO could increase reactive oxidative species that stabilize HIF-1α; and NO may directly nitrosylate cysteine residues on HIF-1α that prevent its degradation.[66,68] Evidence that VEGF-A is a direct target of HIF-1α is well documented.[63,67,69] However, in the context of CNS diseases, Argaw et. al reported that *GfapCre:Hif1a*$^{fl/fl}$ mice displayed insignificant changes in VEGF-A expression or vascular permeability in murine Multiple Sclerosis models.[10] But these findings assessed the role of HIF-1α in CNS models of inflammation and did not investigate the ability of astrocytic HIF-1α to induce VEGF-A expression in models of ischemia or vascular dysfunction where NO levels are augmented.[70] In fact, we show that NO donors (DETA NONOate) were sufficient to induce dramatic increases in VEGF-A and β-gal expression in primary astrocytes of *Vegfa*$^{tm1.1Nagy}$ mice. Moreover, Brix et. al[65] reported that endothelial cells, not astrocytes or neurons, represented the main source of NO that stabilizes astrocytic HIF-1α. Consistent with these findings, we show that expression of astrocyte-derived VEGF-A is dependent on elevated NO production by eNOS. CCM has been characterized as an endothelial cell-autonomous disease, marked by changes in the endothelium due to the loss of *KRIT1*, *CCM2*, or *PDCD10*.[38,71] Our findings that endothelial-

derived NO can stabilize astrocytic HIF-1α to induce the expression of VEGF suggests that CCMs also involve non-cell-autonomous signaling.

Astrocyte-derived VEGF promotes vascular permeability and can contribute to the exacerbation of CCM. In the CNS, VEGF is capable of disrupting the expression of interendothelial junctions claudin-5 and occludin,[47] and has been shown to disrupt VE-cadherin stabilization, resulting in vascular permeability.[13] Previous cases report elevated VEGF expression in the lesions and serum of CCM patients.[57,62] Our findings demonstrate that the elevated expression of VEGF in CCM may be produced by astrocytes. This result augments previous studies in the lab reporting that the loss of KRIT1 increases VEGF expression through the regulation of β-catenin signaling in endothelial cells,[45,46] indicating that multiple mechanisms are likely involved in the upregulation of VEGF during CCM. Furthermore, astrocyte-derived VEGF has been implicated in BBB disruption for other inflammatory CNS diseases.[10,47,59] Consistent with these findings, this study showed for the first time that astrocytes release soluble secreted factors that can contribute to the pathology of CCM. Thus, these findings indicate that increased VEGF signaling may contribute to the exacerbation of CCM.

This study implicates that CNS-resident cells, such as astrocytes, could promote and contribute to the physiological changes that lead to CCM. New studies are needed to investigate other astrocyte HIF-1α target genes that are regulated and to evaluate the possibility of other molecular mechanisms involved in cross-talk between the endothelium and astrocytes during CCM. In addition, the laboratory recently crossed *Pdgfb-iCreERT2; Pdcd10$^{fl/f}$;Nos3$^{-/-}$* mice with *Vegfa$^{tm1.1Nagy}$* mice to detect β-gal expression (VEGF) in the lesions of *Pdcd10^{ECKO};Nos3$^{+/-}$; Vegfa$^{tm1.1Nagy}$* and *Pdcd10^{ECKO};Nos3$^{-/-}$; Vegfa$^{tm1.1Nagy}$* mice. Future work using these mouse models

will allow us to assess if eNOS deficiency leads to altered VEGF-A expression and CCM development *in vivo*.

5. References

1. Andreone BJ, Lacoste B, Gu C. Neuronal and Vascular Interactions. *Annu Rev Neurosci*. 2015. doi:10.1146/annurev-neuro-071714-033835.

2. Cipolla M. Anatomy and Ultrastructure. In: *The Cerebral Circulation*. San Rafael: Morgan & Claypool Life Sciences; 2009.

3. Abbott NJ, Rönnbäck L, Hansson E. Astrocyte–endothelial interactions at the blood–brain barrier. *Nat Rev Neurosci*. 2006. 7(1):41-53. doi:10.1038/nrn1824.

4. Duvernoy HM, Delon S, Vannson JL. Cortical blood vessels of the human brain. *Brain Res Bull*. 1981. 7(5):519-579. doi:https://doi.org/10.1016/0361-9230(81)90007-1.

5. Ribatti D, Nico B, Crivellato E, Artico M. Development of the blood-brain barrier: A historical point of view. *Anat Rec Part B New Anat*. 2006. 289B(1):3-8. doi:10.1002/ar.b.20087.

6. Iadecola C. The Neurovascular Unit Coming of Age: A Journey through Neurovascular Coupling in Health and Disease. *Neuron*. 2017. 96(1):17-42. doi:10.1016/J.NEURON.2017.07.030.

7. Zhao Z, Nelson AR, Betsholtz C, Zlokovic B V. Establishment and Dysfunction of the Blood-Brain Barrier. *Cell*. 2015. 163(5):1064-1078. doi:10.1016/j.cell.2015.10.067.

8. Andreone BJ, Lacoste B, Gu C. Neuronal and Vascular Interactions. *Annu Rev Neurosci*. 2015. 38(1):25-46. doi:10.1146/annurev-neuro-071714-033835.

9. Sweeney MD, Zhao Z, Montagne A, Nelson AR, Zlokovic B V. Blood-Brain Barrier: From Physiology to Disease and Back. *Physiol Rev*. 2019. 99(1):21-78. doi:10.1152/physrev.00050.2017.

10. Argaw AT, Asp L, Zhang J, Navrazhina K, Pham T, Mariani JN, Mahase S, Dutta DJ, Seto J, Kramer EG, Ferrara N, Sofroniew M V., John GR. Astrocyte-derived VEGF-A drives blood-brain barrier disruption in CNS inflammatory disease. *J Clin Invest*. 2012. 122(7):2454-2468. doi:10.1172/JCI60842.

11. Daneman R, Prat A. The blood-brain barrier. *Cold Spring Harb Perspect Biol*. 2015. 7(1):a020412-a020412. doi:10.1101/cshperspect.a020412.

12. Obermeier B, Verma A, Ransohoff RM. Chapter 3 - The blood–brain barrier. In: Pittock SJ, Vincent A, eds. *Autoimmune Neurology*. Vol 133. Handbook of Clinical Neurology. Elsevier; 2016:39-59. doi:https://doi.org/10.1016/B978-0-444-63432-0.00003-7.

13. Dejana E, Orsenigo F, Lampugnani MG. The role of adherens junctions and VE-cadherin in the control of vascular permeability. *J Cell Sci*. 2008. 121(13):2115 LP-2122. doi:10.1242/jcs.017897.

14. Pardridge WM. Blood–brain barrier endogenous transporters as therapeutic targets: a new model for small molecule CNS drug discovery. *Expert Opin Ther Targets*. 2015. 19(8):1059-1072. doi:10.1517/14728222.2015.1042364.

15. Hall CN, Reynell C, Gesslein B, Hamilton NB, Mishra A, Sutherland BA, O'Farrell FM, Buchan AM, Lauritzen M, Attwell D. Capillary pericytes regulate cerebral blood flow in health and disease. *Nature*. 2014. 508:55. https://doi.org/10.1038/nature13165.

16. Armulik A, Genové G, Mäe M, Nisancioglu MH, Wallgard E, Niaudet C, He L, Norlin J, Lindblom P, Strittmatter K, Johansson BR, Betsholtz C. Pericytes regulate the blood–brain barrier.

Nature. 2010. 468:557. https://doi.org/10.1038/nature09522.

17. Leybaert L. Neurobarrier Coupling in the Brain: A Partner of Neurovascular and Neurometabolic Coupling? *J Cereb Blood Flow Metab*. 2005. 25(1):2-16. doi:10.1038/sj.jcbfm.9600001.

18. Nag S. Morphology and Properties of Astrocytes. In: Nag S, ed. *The Blood-Brain and Other Neural Barriers: Reviews and Protocols*. Totowa, NJ: Humana Press; 2010:69-100. doi:10.1007/978-1-60761-938-3_3.

19. Mathiisen TM, Lehre KP, Danbolt NC, Ottersen OP. The perivascular astroglial sheath provides a complete covering of the brain microvessels: An electron microscopic 3D reconstruction. *Glia*. 2010. 58(9):1094-1103. doi:10.1002/glia.20990.

20. McCaslin AFH, Chen BR, Radosevich AJ, Cauli B, Hillman EMC. In vivo 3D morphology of astrocyte-vasculature interactions in the somatosensory cortex: implications for neurovascular coupling. *J Cereb Blood Flow Metab*. 2011. 31(3):795-806. doi:10.1038/jcbfm.2010.204.

21. Abbott NJ, Patabendige AAK, Dolman DEM, Yusof SR, Begley DJ. Structure and function of the blood–brain barrier. *Neurobiol Dis*. 2010. 37(1):13-25. doi:https://doi.org/10.1016/j.nbd.2009.07.030.

22. Buffo A, Rolando C, Ceruti S. Astrocytes in the damaged brain: Molecular and cellular insights into their reactive response and healing potential. *Biochem Pharmacol*. 2010. 79(2):77-89. doi:https://doi.org/10.1016/j.bcp.2009.09.014.

23. Zlokovic B V. The Blood-Brain Barrier in Health and Chronic Neurodegenerative Disorders. *Neuron*. 2008. 57(2):178-201. doi:https://doi.org/10.1016/j.neuron.2008.01.003.

24. Grammas P. Neurovascular dysfunction, inflammation and endothelial activation: Implications for the pathogenesis of Alzheimer's disease. *J Neuroinflammation*. 2011. 8(1):26. doi:10.1186/1742-2094-8-26.

25. Rigamonti D, Hadley MN, Drayer BP, Johnson PC, Hoenig-Rigamonti K, Knight JT, Spetzler RF. Cerebral Cavernous Malformations. *N Engl J Med*. 1988. 319(6):343-347. doi:10.1056/NEJM198808113190605.

26. Keep RF, Zhou N, Xiang J, Andjelkovic A V., Hua Y, Xi G. Vascular disruption and blood-brain barrier dysfunction in intracerebral hemorrhage. *Fluids Barriers CNS*. 2014. 11(1). doi:10.1186/2045-8118-11-18.

27. Robert J. Singer. Cerebral Cavernous Malformation (CCM) | Cerebrovascular Disease and Stroke Program | Dartmouth-Hitchcock. https://www.dartmouth-hitchcock.org/cerebrovascular/cerebral-cavernous-malformation-ccm.html. Published 2014. Accessed June 3, 2019.

28. Labauge P, Denier C, Bergametti F, Tournier-Lasserve E. Genetics of cavernous angiomas. *Lancet Neurol*. 2007. 6(3):237-244. doi:10.1016/S1474-4422(07)70053-4.

29. Ene C, Kaul A, Kim L. Chapter 21 - Natural history of cerebral cavernous malformations. In: Spetzler RF, Moon K, Almefty RO, eds. *Arteriovenous and Cavernous Malformations*. Vol 143. Handbook of Clinical Neurology. Elsevier; 2017:227-232. doi:https://doi.org/10.1016/B978-0-444-63640-9.00021-7.

30. Flemming KD, Graff-Radford J, Aakre J, Kantarci K, Lanzino G, Brown RD, Mielke MM, Roberts RO, Kremers W, Knopman DS, Petersen RC, Jack CR. Population-based prevalence of cerebral cavernous malformations in older adults: Mayo clinic study of aging. *JAMA Neurol*. 2017. 74(7):801-805. doi:10.1001/jamaneurol.2017.0439.

31. Ding D, Starke RM, Crowley RW, Liu KC. Surgical Approaches for Symptomatic Cerebral Cavernous Malformations of the Thalamus and Brainstem. *J Cerebrovasc Endovasc Neurosurg*. 2017. 19(1):19-35. doi:10.7461/jcen.2017.19.1.19.

32. Boulday G, Rudini N, Maddaluno L, Blécon A, Arnould M, Gaudric A, Chapon F, Adams RH, Dejana E, Tournier-Lasserve E. Developmental timing of CCM2 loss influences cerebral cavernous malformations in mice. *J Exp Med*. 2011. 208(9):1835 LP-1847. doi:10.1084/jem.20110571.

33. Lopez-Ramirez MA, Pham A, Girard R, Wyseure T, Hale P, Yamashita A, Koskimäki J, Polster S, Saadat L, Romero IA, Esmon CT, Lagarrigue F, Awad IA, Mosnier LO, Ginsberg MH. Cerebral cavernous malformations form an anticoagulant vascular domain. *Blood*. 2018. 133(3). doi:10.1182/blood-2018-06-856062.

34. Laberge-le Couteulx S, Jung HH, Labauge P, Houtteville JP, Lescoat C, Cecillon M, Marechal E, Joutel A, Bach JF, Tournier-Lasserve E. Truncating mutations in CCM1, encoding KRIT1, cause hereditary cavernous angiomas. *Nat Genet*. 1999. 23(2):189-193. doi:10.1038/13815.

35. Bergametti F, Denier C, Labauge P, Arnoult M, Boetto S, Clanet M, Coubes P, Echenne B, Ibrahim R, Irthum B, Jacquet G, Lonjon M, Moreau JJ, Neau JP, Parker F, Tremoulet M, Tournier-Lasserve E, Neurochirurgie SF de. Mutations within the programmed cell death 10 gene cause cerebral cavernous malformations. *Am J Hum Genet*. 2005. 76(1):42-51. doi:10.1086/426952.

36. Lopez-Ramirez MA, Fonseca G, Zeineddine HA, Girard R, Moore T, Pham A, Cao Y, Shenkar R, de Kreuk B-J, Lagarrigue F, Lawler J, Glass CK, Awad IA, Ginsberg MH. Thrombospondin1 (TSP1) replacement prevents cerebral cavernous malformations. *J Exp Med*. 2017. 214(11). doi:10.1084/jem.20171178.

37. Plummer NW, Zawistowski JS, Marchuk DA. Genetics of cerebral cavernous malformations. *Curr Neurol Neurosci Rep*. 2005. 5(5):391-396. doi:10.1007/s11910-005-0063-7.

38. Scimone C, Donato L, Marino S, Alafaci C, D'Angelo R, Sidoti A. Vis-à-vis: a focus on genetic features of cerebral cavernous malformations and brain arteriovenous malformations pathogenesis. *Neurol Sci*. 2018. 40(2):243-251. doi:10.1007/s10072-018-3674-x.

39. Yoruk B, Gillers BS, Chi NC, Scott IC. Ccm3 functions in a manner distinct from Ccm1 and Ccm2 in a zebrafish model of CCM vascular disease. *Dev Biol*. 2012. 362(2):121-131. doi:https://doi.org/10.1016/j.ydbio.2011.12.006.

40. Renz M, Otten C, Faurobert E, Rudolph F, Zhu Y, Boulday G, Duchene J, Mickoleit M, Dietrich A-C, Ramspacher C, Steed E, Manet-Dupé S, Benz A, Hassel D, Vermot J, Huisken J, Tournier-Lasserve E, Felbor U, Sure U, Albiges-Rizo C, Abdelilah-Seyfried S. Regulation of β1 Integrin-Klf2-Mediated Angiogenesis by CCM Proteins. *Dev Cell*. 2015. 32(2):181-190. doi:10.1016/j.devcel.2014.12.016.

41. Zhou Z, Rawnsley DR, Goddard LM, Pan W, Cao X-J, Jakus Z, Zheng H, Yang J, Arthur JSC, Whitehead KJ, Li D, Zhou B, Garcia BA, Zheng X, Kahn ML. The Cerebral Cavernous Malformation Pathway Controls Cardiac Development via Regulation of Endocardial MEKK3 Signaling and KLF Expression. *Dev Cell*. 2015. 32(2):168-180. doi:https://doi.org/10.1016/j.devcel.2014.12.009.

42. Draheim KM, Fisher OS, Boggon TJ, Calderwood DA. Cerebral cavernous malformation proteins at a glance. *J Cell Sci*. 2014. 127(4):701-707. doi:10.1242/jcs.138388.

43. Bravi L, Malinverno M, Pisati F, Rudini N, Cuttano R, Pallini R, Martini M, Larocca LM, Locatelli M, Levi V, Bertani GA, Dejana E, Lampugnani MG. Endothelial Cells Lining Sporadic Cerebral Cavernous Malformation Cavernomas Undergo Endothelial-to-Mesenchymal Transition. *Stroke*. 2016. 47(3):886-890. doi:10.1161/STROKEAHA.115.011867.

44. Stockton RA, Shenkar R, Awad IA, Ginsberg MH. Cerebral cavernous malformations proteins inhibit Rho kinase to stabilize vascular integrity. *J Exp Med*. 2010. 207(4):881 LP-896. doi:10.1084/jem.20091258.

45. Glading AJ, Ginsberg MH. Rap1 and its effector KRIT1/CCM1 regulate β-catenin signaling. *Dis Model & Mech*. 2010. 3(1-2):73 LP-83. doi:10.1242/dmm.003293.

46. DiStefano P V., Kuebel JM, Sarelius IH, Glading AJ. KRIT1 protein depletion modifies endothelial cell behavior via increased vascular endothelial growth factor (VEGF) Signaling. *J Biol Chem*. 2014. doi:10.1074/jbc.M114.582304.

47. Argaw AT, Gurfein BT, Zhang Y, Zameer A, John GR. VEGF-mediated disruption of endothelial CLN-5 promotes blood-brain barrier breakdown. *Proc Natl Acad Sci*. 2009. 106(6):1977 LP-1982. doi:10.1073/pnas.0808698106.

48. Fujimura M, Watanabe M, Shimizu H, Tominaga T. Expression of matrix metalloproteinases (MMPs) and tissue inhibitor of metalloproteinase (TIMP) in cerebral cavernous malformations: immunohistochemical analysis of MMP-2, -9 and TIMP-2. *Acta Neurochir (Wien)*. 2007. 149(2):179-183. doi:10.1007/s00701-006-0929-8.

49. Wüstehube J, Bartol A, Liebler SS, Brütsch R, Zhu Y, Felbor U, Sure U, Augustin HG, Fischer A. Cerebral cavernous malformation protein CCM1 inhibits sprouting angiogenesis by activating DELTA-NOTCH signaling. *Proc Natl Acad Sci*. 2010. doi:10.1073/pnas.1000132107.

50. Maddaluno L, Rudini N, Cuttano R, Bravi L, Giampietro C, Corada M, Ferrarini L, Orsenigo F, Papa E, Boulday G, Tournier-Lasserve E, Chapon F, Richichi C, Retta SF, Lampugnani MG, Dejana E. EndMT contributes to the onset and progression of cerebral cavernous malformations. *Nature*. 2013. doi:10.1038/nature12207.

51. Orsenigo F, Papa E, Boulday G, Tournier-lasserve E, Chapon F, Richichi C. EndMT contributes to the onset and progression of cerebral cavernous malformations. *Nature*. 2013. 498(7455):492-496. doi:10.1038/nature12207.

52. Zhou Z, Tang AT, Wong WY, Bamezai S, Goddard LM, Shenkar R, Zhou S, Yang J, Wright AC, Foley M, Arthur JSC, Whitehead KJ, Awad IA, Li DY, Zheng X, Kahn ML. Cerebral cavernous malformations arise from endothelial gain of MEKK3-KLF2/4 signalling. *Nature*. 2016. 532(7597):122-126. doi:10.1038/nature17178.

53. Cuttano R, Rudini N, Bravi L, Corada M, Giampietro C, Papa E, Morini MF, Maddaluno L, Baeyens N, Adams RH, Jain MK, Owens GK, Schwartz M, Lampugnani MG, Dejana E. KLF4 is a key determinant in the development and progression of cerebral cavernous malformations. *EMBO Mol Med*. 2016. 8(1):6 LP-24. doi:10.15252/emmm.201505433.

54. Koskimäki J, Girard R, Li Y, Saadat L, Zeineddine HA, Lightle R, Moore T, Lyne S, Avner K, Shenkar R, Cao Y, Shi C, Polster SP, Zhang D, Carrión-Penagos J, Romanos S, Fonseca G, Lopez-Ramirez MA, Chapman EM, Popiel E, Tang AT, Akers A, Faber P, Andrade J, Ginsberg M, Derry WB, Kahn ML, Marchuk DA, Awad IA. Comprehensive transcriptome analysis of cerebral cavernous malformation across multiple species and genotypes. *JCI Insight*. 2019. 4(3). doi:10.1172/jci.insight.126167.

55. Durán WN, Breslin JW, Sánchez FA. The NO cascade, eNOS location, and microvascular permeability. *Cardiovasc Res*. 2010. 87(2):254-261. doi:10.1093/cvr/cvq139.

56. Livak KJ, Schmittgen TD. Analysis of Relative Gene Expression Data Using Real-Time Quantitative PCR and the 2−ΔΔCT Method. *Methods*. 2001. 25(4):402-408. doi:https://doi.org/10.1006/meth.2001.1262.

57. Jung K-H, Chu K, Jeong S-W, Park H-K, Bae H-J, Yoon B-W. Cerebral Cavernous Malformations With Dynamic and Progressive Course: Correlation Study With Vascular Endothelial Growth Factor. *JAMA Neurol*. 2003. 60(11):1613-1618. doi:10.1001/archneur.60.11.1613.

58. Claxton S, Kostourou V, Jadeja S, Chambon P, Hodivala-Dilke K, Fruttiger M. Efficient, inducible Cre-recombinase activation in vascular endothelium. *genesis*. 2008. 46(2):74-80. doi:10.1002/dvg.20367.

59. Zhang R, Wang L, Zhang L, Chen J, Zhu Z, Zhang Z, Chopp M. Nitric Oxide Enhances Angiogenesis via the Synthesis of Vascular Endothelial Growth Factor and cGMP After Stroke in the Rat. *Circ Res*. 2003. 92(3):308-313. doi:10.1161/01.RES.0000056757.93432.8C.

60. Miquerol L, Gertsenstein M, Harpal K, Rossant J, Nagy A. Multiple Developmental Roles of VEGF Suggested by a LacZ-Tagged Allele. *Dev Biol*. 1999. 212(2):307-322. doi:https://doi.org/10.1006/dbio.1999.9355.

61. Burn SF. Detection of $β$-Galactosidase Activity: X-gal Staining. In: Michos O, ed. *Kidney Development: Methods and Protocols*. Totowa, NJ: Humana Press; 2012:241-250. doi:10.1007/978-1-61779-851-1_21.

62. Abe T, Morishige M, Ooba H, Kamida T, Fujiki M, Kobayashi H, Sakoda T, Kimba Y. The association between high VEGF levels and multiple probable punctuate cavernous malformations. *Acta Neurochir (Wien)*. 2009. 151(7):855. doi:10.1007/s00701-009-0410-6.

63. Shi Q, Liu X, Wang N, Zheng X, Fu J, Zheng J. Nitric oxide from brain microvascular endothelial cells may initiate the compensatory response to mild hypoxia of astrocytes in a hypoxia-inducible factor-1α dependent manner. *Am J Transl Res*. 2016. 8(11):4735-4749. https://www.ncbi.nlm.nih.gov/pubmed/27904676.

64. Guix FX, Uribesalgo I, Coma M, Muñoz FJ. The physiology and pathophysiology of nitric oxide in the brain. *Prog Neurobiol*. 2005. 76(2):126-152. doi:https://doi.org/10.1016/j.pneurobio.2005.06.001.

65. Brix B, Mesters JR, Pellerin L, Jöhren O. Endothelial Cell-Derived Nitric Oxide Enhances Aerobic Glycolysis in Astrocytes via HIF-1α-Mediated Target Gene Activation. *J Neurosci*. 2012. 32(28):9727-9735. doi:10.1523/JNEUROSCI.0879-12.2012.

66. Olson N, van der Vliet A. Interactions between nitric oxide and hypoxia-inducible factor signaling pathways in inflammatory disease. *Nitric Oxide*. 2011. 25(2):125-137. doi:https://doi.org/10.1016/j.niox.2010.12.010.

67. Sandau KB, Fandrey J, Brüne B. Accumulation of HIF-1α under the influence of nitric oxide. *Blood*. 2001. 97(4):1009 LP-1015. http://www.bloodjournal.org/content/97/4/1009.abstract.

68. Schleicher M, Yu J, Murata T, Derakhshan B, Atochin D, Qian L, Kashiwagi S, Di Lorenzo A, Harrison KD, Huang PL, Sessa WC. The Akt1-eNOS Axis Illustrates the Specificity of Kinase-Substrate Relationships in Vivo. *Sci Signal*. 2009. 2(82):ra41--ra41. doi:10.1126/scisignal.2000343.

69. Choi YK, Kim C-K, Lee H, Jeoung D, Ha K-S, Kwon Y-G, Kim K-W, Kim Y-M. Carbon Monoxide Promotes VEGF Expression by Increasing HIF-1α Protein Level via Two Distinct Mechanisms, Translational Activation and Stabilization of HIF-1α Protein. *J Biol Chem* . 2010. 285(42):32116-32125. doi:10.1074/jbc.M110.131284.

70. Endres M, Laufs U, Liao JK, Moskowitz MA. Targeting eNOS for stroke protection. *Trends Neurosci*. 2004. 27(5):283-289. doi:https://doi.org/10.1016/j.tins.2004.03.009.

71. Hogan BM, Bussmann J, Schulte-Merker S, Wolburg H. ccm1 cell autonomously regulates endothelial cellular morphogenesis and vascular tubulogenesis in zebrafish . *Hum Mol Genet*. 2008. 17(16):2424-2432. doi:10.1093/hmg/ddn142.